Accepted Manuscript

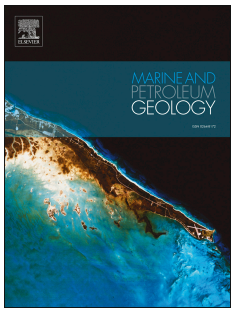

Fracture patterns and petrophysical properties of carbonates undergoing regional folding: A case study from Kurdistan, N Iraq

Abdullah Awdal, David Healy, G. Ian Alsop

PII: S0264-8172(15)30165-3

DOI: 10.1016/j.marpetgeo.2015.12.017

Reference: JMPG 2425

To appear in: *Marine and Petroleum Geology*

Received Date: 24 September 2014

Revised Date: 25 October 2015

Accepted Date: 20 December 2015

Please cite this article as: Awdal, A., Healy, D., Alsop, G.I., Fracture patterns and petrophysical properties of carbonates undergoing regional folding: A case study from Kurdistan, N Iraq, *Marine and Petroleum Geology* (2016), doi: 10.1016/j.marpetgeo.2015.12.017.

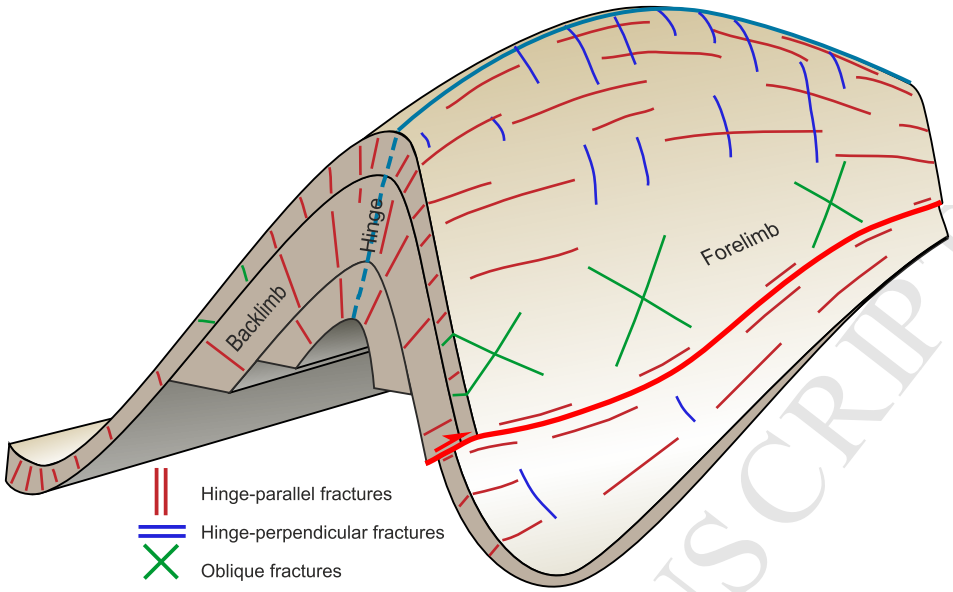

Fracture patterns and petrophysical properties of carbonates undergoing regional folding: A case study from Kurdistan, N Iraq

Abdullah Awdal[1], David Healy[2], G. Ian Alsop[2]

[1] GeoScience Limited, Falmouth Business Park, Bickland Water Road, Falmouth, Cornwall, TR11 4SZ, United Kingdom

[2] Department of Geology and Petroleum Geology, School of Geosciences, University of Aberdeen, Aberdeen, AB24 3UE, United Kingdom

*Corresponding author (email: awdal@geoscience.co.uk)

Abstract

The Zagros-Taurus fold and thrust belt hosts a prolific hydrocarbon system. Most hydrocarbon reserves are stored in naturally fractured reservoirs and such fracture systems can therefore have a significant impact on reservoir performance. Fractures are one of the most important paths for fluid flow in carbonate reservoirs, and industrial geoscientists and engineers therefore need to understand and study fracture patterns in order to optimise hydrocarbon production. The observed fracture patterns in outcrops may have implications on fluid flow and reservoir modelling in subsurface reservoirs, and we have therefore undertaken a case study of fracturing associated with regional folding in Iraqi Kurdistan. In this area, some exploration wells currently target Upper Triassic dolostones (Kurra Chine Formation) and/or Lower Jurassic limestones and dolomitised limestones (Sehkaniyan Formation). In both units hydrocarbon production comes mainly from secondary porosity created by dolomitisation, dissolution and fracturing. Both formations have undergone multiple phases of

deformation associated with burial, uplift, folding and thrusting. We investigate some fracture pattern characteristics and some petrophysical properties of these units using selected outcrops around the Gara, Ora and Ranya anticlines that form folds directly traceable for 25-70 km. Our outcrop data is compared with subsurface fracture and petrophysical datasets reported from wells in the nearby Shaikhan and Swara Tika Fields. The 1-2-3D fracture attributes collected from outcrops are fracture orientation, type, spacing, intensity, length and cross-cutting and abutting relationships. Fracture orientations show a clear relationship to the local fold axis in both the outcrop and subsurface, although in some cases they appear to relate more to the present day *in-situ* maximum horizontal stress direction or local strike-slip faulting. Three stages of fracturing are proposed: pre-folding, early-folding and post-folding fractures. In addition, we report petrophysical properties - porosity, permeability and acoustic velocity of both the Kurra Chine and Sehkaniyan formations in relation to their structural position within folds and faults and stratigraphic level. The highest porosities and permeabilities are recorded in the hinges and backlimbs of the Gara Anticline. The best reservoir quality (highest porosity and permeability) is often found in areas associated with replacement dolomite i.e. solution vugs and intercrystalline porosity. The Kurra Chine Formation displays similar trends in velocity-porosity data at both outcrop and the subsurface. However, the Sehkaniyan Formation displays lower acoustic velocity for a given porosity at outcrop compared to the subsurface.

Keywords: fracture; petrophysical properties; Zagros; Kurdistan; Iraq

1. Introduction

Fractures are one of the most important paths for fluid flow in carbonate reservoirs. Natural fracture systems can have a dramatic impact on reservoir performance and can act as permeable flow conduits or as baffles and seals (Bourne et al., 2000; Agosta, 2008). Outcrop analogue studies can improve understanding of some aspects of fracture distributions and their influence on fluid flow in fractured reservoirs (e.g. Antonellini and Mollema, 2000; Aydin, 2000; Nelson, 2001; Stephenson et al., 2007; Lacombe et al., 2011) and their influence on petrophysical properties such as porosity and velocity (Nemati and Pezeshk, 2005; Healy et al., 2015). However, the scaled outcrop data should be used with care in order to improve reservoir modelling and constrain uncertainties (Sharp et al., 2006; Wennberg et al., 2006; Barr et al., 2007; Lapponi et al., 2011). For example, the processes that have affected fracture generation at outcrop such as uplift, gas expansion, and erosion would not have occurred at depth, and is not therefore relevant to deeper reservoirs.

The Zagros mountain belt is a prolific petroleum province with several producing oil and gas fields (e.g. Cooper, 2007). Numerous outcrop analogue studies of fractured reservoirs have been undertaken, describing fracture patterns in the Zagros fold and thrust belt, especially in Iran (e.g. Wennberg et al., 2006; Ahmadhadi et al., 2008; Stephenson et al., 2007; Casini et al., 2011; Lacombe et al., 2011; Tavani et al., 2011). Reservoirs are mainly fractured carbonates developed at a variety of stratigraphic levels. Many studies show that fracture pattern is controlled by mechanical stratigraphy and petrophysical properties such as porosity (e.g. McQuillan, 1973; Huang and Angelier, 1989; Underwood et al., 2003; Nemati and Pezeshk, 2005; Wennberg et al., 2006). In a study of folded carbonate units in SW Iran, Wennberg et al. (2006) suggest that the spatial distribution of fractures is a multivariate problem, where fracture attributes such as orientation, length, spacing and apertures are functions of position within the fold, sedimentary texture and mechanical bed thickness.

Fracture patterns could also be controlled by the evolution of fluid pressures during burial and evolution of the stress field during unroofing (uplifting).

The fracture patterns and petrophysical properties of potential carbonate reservoirs are investigated within Iraqi Kurdistan, as represented by the Sehkaniyan Formation (Lower Jurassic) and the Kurra Chine Formation (Upper Triassic) (Figs. 1a, 1b, 2). The outcrop fracture datasets are mainly collected in E-W trending structures and nearby subsurface oil fields. These localities are chosen because of the outcrop exposures of the studied units. In this paper, we focus on the potential control that regional anticlines may exert on the fracture patterns and petrophysical properties of folded and fractured carbonates. Reservoir units are analysed in outcrops around regional folds comprising the Gara, Ora and Ranya anticlines, and in the subsurface within the Shaikhan and Swara Tika oil fields (Figs. 1a, b). The Gara Anticline is studied because it is regarded as viable outcrop analogue to the nearby Shaikhan and Swara Tika fields, whereas the Ora and Ranya anticlines were selected as supplementary outcrops as they exhibit good exposures of the Kurra Chine and Sehkaniyan formations, respectively.

2. Geological setting

2.1. Tectonics

The Zagros-Taurus fold and thrust belt is situated along the NE margin of the Arabian Plate. It has developed as a consequence of the oblique collision between the Arabian and the Eurasian plates (Homke et al., 2004; Homke et al., 2009), reflecting gradual closure of the NeoTethys Ocean mainly during Late Cretaceous–Cenozoic times (Talbot and Alavi, 1996). The onset of Arabian–Eurasian plate collision, and associated folding and thrusting of the Zagros Orogeny started in the Oligocene and is still active (Fard et al., 2006). The Zagros

orogenic belt in Kurdistan can be divided into five distinct structural zones, that from the NE hinterland to the SW foreland, and are named the: Zagros Suture, Imbricated Zone, Highly Folded Zone, Foothill Zone and Mesopotamian Foreland Basin (Jassim and Goff, 2006) (Fig. 1a). The Imbricate and Highly Folded zones are characterised by major surface-breaching, mainly SW-verging thrust-related anticlines, whereas major folds above blind thrusts characterise the Foothill Zone (Awdal et al., 2013). The orientation of fold axes in the study area varies from NW-SE Zagros (e.g. Ranya Anticline) to WNW-ESE Taurus trends (e.g. Gara and Swara Tika anticlines) (Fig. 1b).

The structural style of the Zagros-Taurus fold and thrust belt in Iraqi Kurdistan is characterised by thin- and thick-skinned tectonics (Kubli and McKenna, 2013), and is segmented due to the interaction of the exposure level and variations in decollement levels along strike (Granath and Odell, 2014). The stratigraphy is dominated by competent to incompetent carbonate units interbedded with detached intervals of incompetent siliciclastic rocks often bearing evaporite beds. The main thin-skinned detachment levels occur in the Lower Fars (Neogene), the Gercus-Kolosh (Palaeogene), the Jurassic, and the Baluti (Upper Triassic). In addition, thick-skinned detachment levels are likely to occur at one or more deeper levels within the Palaeozoic (e.g. Ora Shale) (Granath and Odell, 2014). This stratigraphic architecture sets up a structural style composed of ramps cutting across the competent carbonates, and flats running along incompetent units (Al-Breefkani, 2008; Granath and Odell, 2014). Duplexes are formed by a group of ramps and comprise narrow repeated fault slices that build structural relief. The floor thrust is the lower detachment below the duplex, whereas a possible passive roof fault is the upper detachment which isolates the duplex from an overlying carapace of less deformed rocks (Al-Breefkani, 2008; Granath and Odell, 2014). In south-eastern Iraqi Kurdistan, the surface structures are decoupled from the more complex subsurface structures by multiple thrust sheets. Folding, faulting and uplift of

early formed thrust sheets took place during progressive structural thickening of the orogenic wedge. The orogenic wedge itself is characterised by a stack of nappes and hinterland-dipping, connecting splay duplexes (Banks, 2013). Basement blocks are possibly involved in the thick-skinned tectonic phase and there is most likely reactivation along some of the pre-existing Late Cretaceous extensional faults (Kubli and McKenna, 2013).

Gara and Shaikhan are asymmetrical double-plunging anticlines with N-directed vergence and WNW-ESE and E-W orientated fold axes, respectively. Conversely, Swara Tika is an asymmetrical double-plunging anticline (i.e. pericline) with S-directed vergence and a WNW-ESE orientated fold axis. The Ora Anticline is an asymmetrical, cylindrical and open fold with S-directed vergence and E-W orientated fold axis. The Ranya Anticline is asymmetrical with NE-directed vergence and a NW-SE oriented fold axis. The Gara, Ranya, Shaikhan and Swara Tika anticlines are all located within the Highly Folded Zone, whereas the Ora Anticline is positioned within the Imbricated Zone of the Zagros-Taurus fold and thrust belt. These anticlines display a range of geometrical similarities and differences, in terms of structural styles and fractured reservoir characteristics.

2.2. Stratigraphy

The studied stratigraphic units are the Upper Triassic Kurra Chine and Lower Jurassic Sehkaniyan formations (Figs. 1b, 2). Both units are considered as good reservoirs in recent discoveries within Kurdistan, and contain hydrocarbons within the Shaikhan, Atrush and Swara Tika fields (Figs. 1a, b). The subsurface equivalents to the Sehkaniyan Formation in Iraq are the Alan, Mus and Adaiyah formations (van Bellen et al., 1959) (Fig. 2).

The Kurra Chine Formation was deposited during the Late Triassic within the Kand and Qara Chauq sub-basins of northern Iraq (Sadooni, 1995). The Kurra Chine Formation is

assigned to the Kand Basin (Carnian-Norian) which covers an area of 10,000 km^2 in northern Kurdistan (Sadooni, 1995). Well data indicates a maximum sediment thickness of up to 1000 m in the basin. The thickness is varied in outcrops and this variation is possibly due to dissolution of evaporite beds (Aqrawi et al., 2010). Sedimentation was affected by basement block faulting, the initiation of NeoTethys rifting and by arid and semi-arid climate conditions (Sadooni, 1995). During the Late Triassic, the main tectonic events were passive subsidence and minor extension. The Early Jurassic rocks were continuously deposited over the Triassic rocks (Sissakian, 2013). According to microfacies analysis, the Sehkaniyan Formation was deposited in shallow open and restricted marine facies on a carbonate platform ramp (Jassim and Goff, 2006).

The Kurra Chine Formation is best exposed at its type locality along the northern flank of the Ora Anticline (Figs. 1a, b). Here, the thickness of the unit is 834 m and comprises dolomitised carbonates. On the southern limb of the Ora Anticline, the entire Kurra Chine section is represented by crystalline dolomites and limestones (van Bellen et al., 1959). It crops out in a few other localities such as in the core of the Gara Anticline. At outcrop, the unit consists of alternating thin-bedded and thick-bedded limestones, with intercalations of thick-bedded foetid dolomites showing slump-structures, and of papery shales. Breccia beds at the type section were interpreted as being formed by dissolution and recrystallization of evaporites by meteoric waters (van Bellen et al., 1959). This interpretation is supported by the presence of thick evaporite intervals in the subsurface (Aqrawi et al., 2010). The Kurra Chine Formation was possibly deposited on an epeiric platform, dominated by subtidal to supratidal cycles with the local development of sabkhas (Aqrawi et al., 2010). However, there are well developed black shales reported in some subsurface wells, and these may have been deposited in restricted intrashelf basins such as the Kand Basin (Sadooni, 1995; Aqrawi et al., 2010).

The Sehkaniyan Formation (Lower Jurassic) is exposed in the hinges of many anticlines in Kurdistan, and forms the core of Gara and Ranya anticlines, where it defines an upstanding ridge along the hinge of the Gara Anticline. It is up to 350 m thick and consists of foetid, saccharoidal dolomites and dolomitised limestones. These locally contain chert, and organic and pellety limestones (locally dolomitised), with silicified fossils and pseudo breccias. The breccias were probably formed by the dissolution of evaporites (van Bellen et al., 1959; Aqrawi et al., 2010). The lower part of the Sehkaniyan Formation was deposited in a restricted carbonate platform facies (Aqrawi et al., 2010) while the middle and the upper parts are euxinic (Buday, 1980).

3. Summary of the studied fracture elements

Some fundamental controls on carbonate fracturing are burial, diagenesis, dolomitisation, hydrocarbon fluid expansion, overpressure, proximity to pre-existing faults, evolution of mechanical and fracture stratigraphies, mechanical anisotropy and overburden removal. Therefore, the timing of the numerous fracture generations and the fundamental deformation mechanisms of an evolving fold-thrust belt is crucial. In order to fully discern the evolution of the fracture system, it would require analysis of carbonate sedimentology, paragenesis, fluid evolution, modelling of burial and uplift magnitudes and timing etc. However, this paper is only assessing some aspects of present-day fracture patterns (Table 1). In this paper, joints are the studied fracture type as they are common structures in all study areas. The scope of this paper is narrower than other fracture studies in fold-thrust belts that cover pre-folding joints (Bergbauer and Pollard, 2004), fracture intensity versus mechanical stratigraphy (Wennberg et al., 2006), fracture density and surface curvature (Bergbauer, 2007; Cosgrove, 2015) and the role of mechanical anisotropy and curvature on fracture development (Stephenson et al.,

2007). The current study is time and outcrop constrained compared to these other fracture studies.

Fractures in fold-thrust belts can be generated either pre-folding or post-folding (e.g. Bellahsen et al., 2006; Ameen et al., 2010) (Fig. 3), and can be distinguished using criteria such as relation between fracture orientations and the fold axis, fracture dip angle with respect to bedding, and others. Extensional fractures may develop on the outer arcs of flexural slip folds. In addition, some fractures may not be of the same age as contractional folds. The proposed conceptual model in this study may only be applicable to the studied anticlines and not beyond. Because folded structures are the focus of this paper, the fractured carbonates are studied at different structural positions of the folds, but not further away from these folds. The solution of limestones and evaporites may reduce fracture width, and hence reduce connectivity and permeability. However, dolomitisation enhances matrix porosity due to formation of intercrystalline porosity, and when dolomitisation is structurally controlled, it develops good reservoir quality facies in the vicinity of faults and fracture corridors. Faults and fractures act as fluid-migration pathways and they are the main controls on vuggy porosity distribution during deep burial (Lønøy, 2006).

4. Methods and Data

4.1. Outcrop data

Field work was conducted in outcrops of the Kurra Chine and Sehkaniyan formations around the Gara, Ora and Ranya anticlines (Figs. 1a, b). These folds are chosen because of the outcrop exposures of the studied units. Both formations are regarded as fractured reservoir units with hydrocarbon shows in several boreholes in the region. One-dimensional line sampling (scanlines) was used for outcrop data collection, following the methodology of

Priest (1993). This sampling technique requires a well-exposed, bedding surface or planar rock face that is large relative to the size and spacing of the exposed fractures. Each scanline was marked with a measuring tape, and was around 30 m long. In order to reduce the directional sampling bias, the scan lines were set up perpendicular to fractures. The reported fracture data were measured from 15 scanlines on bedding planes at different localities around the Gara, Ora and Ranya anticlines. These localities were carefully chosen in order to collect representative data from different structural positions in each fold, i.e. the forelimb, backlimb and hinge areas of each fold. Data sampled along each scanline includes: fracture spacing, fracture strike and dip, fracture length, fracture type and type of fracture termination (covered, termination in intact rock or fracture tips abutting against other fractures). In order to compare fracture orientations to the local fold axis and investigate if there is a pre-folding fracture family, fractures are back-tilted until associated bedding is restored to the horizontal. Bedding dip removal is required to determine the original set of fractures that could have been subject to a later regional folding event. It is also required to study the relation between pre-folded fracture orientation and the incipient compression or shortening direction of a later formed fold.

Fracture orientation data were graphically presented by using stereograms to describe the fracture surface as planes in 3D, and rose diagrams to illustrate the trend of the fracture strikes in 2D. Furthermore, the sampling bias of fracture densities from directional scanlines was corrected using the Terzaghi correction (Terzaghi, 1965).

4.2. Subsurface data

Subsurface datasets were analysed from the Shaikhan and Swara Tika fields, as they are close to outcrop analogues of the Gara Anticline. Wireline and image log datasets were analysed from the Shaikhan Field (vertical wells SH-1, SH-2 and SH-4) and the Swara Tika Field

(deviated wells ST-1 and ST-2) (Figs. 1a, b). The image logs were calibrated for depth to available drill core by using wireline logs such as spectral gamma ray, density and neutron logs. Fracture dip is measured relative to horizontal, with the formation dip being rather low because the wells are located near the crests of the anticlines.

Image logs provide information about the location and orientation of fractures in the reservoirs. Resistivity borehole images such as Formation Micro Imager (FMI) and Extended Range Micro Imager (XRMI) were used for fracture interpretation in Techlog software (Schlumberger Ltd., 2013). The image log raw and processed data (i.e. DLIS files) are used for fracture interpretation. No depth shift correction was applied to the datasets because the image log depth matched with the wireline depth. Pad images were created and oriented relative to the north of the borehole. Static and dynamic image logs were generated by applying different normalisation to the image. Electrically conductive features appear dark on resistivity images, while electrically resistive features appear bright, and hybrid features appear dark and bright. Natural fractures were manually picked and interpreted as potentially open fractures (conductive features), potentially mineralised fractures (resistive features) and part-open part-mineralised fractures (hybrid features).

In addition, density and sonic logs were used to quantify porosity and acoustic velocity from wells SH-1 and ST-1 using a script written in Matlab software (The MathWorks Inc., 2013). The plotted porosity and acoustic velocity data represent fluid saturated intervals.

4.3. Laboratory work

In order to measure porosity, permeability and acoustic velocity, a total of 65 core plugs measuring 2.54 cm in diameter and varying in length between 2.54 and 5.08 cm were drilled from 57 outcrop samples, collected around the Gara, Ora and Ranya anticlines. All core plugs were initially washed with water and then dried in an oven at 40^{o}C for 24 hours in order to

remove water trapped in pores. Porosity was then measured using helium in a porosimeter. Permeability was measured using nitrogen in a Hassler sleeve permeameter. To investigate the impact of burial depth, core plug permeability was also measured in a confining pressure permeameter using nitrogen gas as pore fluid. All measurements were run at room temperatures ranging between 18-22^{o}C. P-wave velocity was measured using a digital oscilloscope and a pulse generator. For acoustic velocity measurement, a frequency of 100 and 1000 kHz were used. The petrophysical properties of outcrop core plugs were measured under dry sample conditions. It should be noted that these differ from porosity and acoustic velocity data measured from wireline logs, which are considered to be fluid saturated.

We now describe the results of the analysis of fracture patterns and petrophysical properties from each of the outcrop study areas: Gara, Ora and Ranya anticlines, together with the Shaikhan and Swara Tika sub-surface fields.

5. Gara Anticline

The Gara Anticline is located about 55 km east-north-eastwards from Duhok City within the Highly Folded Zone of the Zagros fold and thrust belt (Figs. 1a, b). It is a WNW-ESE trending asymmetrical and double-plunging anticline. The Gara Anticline is a regional fold traceable for 72 km along its length, and is up to 10 km in width as marked by the closure of competent Aqra Formation. The structure verges towards the north, with several local thrust faults displaying top toward the south displacement. The northern flank of the anticline is also cut by several faults that form deep narrow gorges through the Pila Spi, Aqra and Sehkaniyan carbonate formations. The core of the anticline is accessible through the Derash and Garagu Gullies and comprises Kurra Chine, Baluti (Upper Triassic) and Sarki Formations (Lower Jurassic). The dip of stratigraphic units in the northern flank increases gradually towards the

lower stratigraphic levels, with the dip of the Jurassic units abruptly increasing to nearly vertical due to thrust faulting as observed at outcrop.

5.1. Fracture orientation and intensity in the Gara Anticline

Fracture datasets were collected from three localities within the Kurra Chine Formation exposed around the Gara Anticline. These localities are situated in the forelimb (KC-1); hinge (KC-2) and in the backlimb (KC-3) of the fold (Fig. 4a). Fracture attributes such as orientation, intensity and type were measured at each of these localities. Locality KC-1 is positioned north of the axial trace of the Gara Anticline. Bedding dips gently (~22^{o}) towards the north and is considered to form part of the forelimb of the Gara Anticline. Joints and veins are the most common fracture types (Figs. 4b, c). Most fracture dips are sub-perpendicular to bedding, allowing fracture sets to be characterised according to their trend. Four sets of fractures were observed at this locality trending: (i) WNW-ESE; (ii) ENE-WSW; (iii) NNE-SSW and (iv) NE-SW (Fig. 5a). The first two fracture sets dominate the outcrop. Fractures strike NNE-SSW are perpendicular to the fold axis. Fracture intensity or 1D fracture density is the number of fracture intersections per unit length along a scanline, and it is referred to as P10 (m^{-1}) (Dershowitz and Herda, 1992; Aliverti et al., 2003). The measured fracture intensity (P10) at this locality is 5.12 m^{-1}. This intensity value represents all fracture sets. In addition, tectonic stylolites were observed cross cutting other fractures that now contain bitumen.

Locality KC-2 is 2.5 km to the east of locality KC-1 in the hinge zone of the Gara Anticline (Fig. 5a). Bedding is almost horizontal (~5^{o}) reflecting its position at the crest of the anticline. Some fractures are veins that are partially filled with calcite and oriented NNE-SSW. A dominant fracture set striking WNW-ESE was observed in the outcrop (Fig. 5a). Locality KC-3 is about 4 km further east from locality KC-2 and lies on the backlimb of the Gara Anticline. This locality exposes the Kurra Chine Formation (Fig. 4b). Bedding dips

moderately to the south (~48^{o}) and fractures are oriented in NE-SW, NW-SE, N-S and E-W directions (Fig. 5a). Bedding-parallel shear fractures (veins) have been observed at all localities, while bitumen was noted along some fractures, and in particular at locality KC-1. The WNW-ESE fracture set parallels the fold axis while the NNE-SSW set is oriented perpendicular to the fold axis (Fig. 5a).

The Sehkaniyan Formation is a massive carbonate that does not display well defined bedding surfaces or smooth rock faces for fracture studies. Nevertheless, fracture orientation data and rock samples were collected at four localities around the Gara Anticline. These include the forelimb (SK-1, SK-2) and the backlimb (SK-3, SK-4) of the fold (Figs. 5a, b). Fractures in the Sehkaniyan Formation are dominantly oriented E-W and N-S, with a minority of NE-SW and NW-SE orientations (Fig. 5a). The majority of fractures are joints which are sub-perpendicular to the bedding, while others are layer-oblique fractures. In some cases they form conjugate sets whose acute angle is bisected by the shortening direction, such as those at locality SK-2 (Fig. 5a). Hydrocarbon in the form of bitumen has invaded the partly cemented fractures and vugs in the damage zones of thrust faults within the Sehkaniyan Formation (Figs. 4d, e), and will be discussed in more detail in relation to implications for fracture timing. Furthermore, tectonic stylolites were also observed to contain bitumen and cross cut other fractures. This is particularly observed at locality SK-2 within the damage zone of a thrust fault associated with top to the south displacement (Figs. 5a, b).

The observed NNE-SSW fractures strike perpendicular to the fold axis in the Gara Anticline. This fracture set is partially cemented with calcite and is hydrocarbon stained. Another hydrocarbon stained fracture set is observed along and within the damage zone of the E-W striking thrust faults. These observations may have implications for reservoir connectivity in the subsurface. Furthermore, stress release during uplift and weathering are likely to enhance the differences in fracture patterns between the surface and subsurface

anticlines. Fracture patterns at surface can be affected by evolution of the stress field during unroofing (uplifting), whereas fractures may be influenced by evolution of fluid pressures during burial at subsurface condition.

5.2. Petrophysical properties in the Gara Anticline

Helium porosity, nitrogen permeability, confining pressure-permeability and acoustic velocity were measured from core plugs drilled from the outcrop samples. There is a general trend of increasing permeability with increasing porosity (Figs. 6a, b). Porosity-permeability datasets for both the Kurra Chine and Sehkaniyan reservoir units were also classified relative to their structural positions around the Gara Anticline (Figs. 6c, d). Within the Sehkaniyan Formation exposed around the Gara Anticline, a range of porosities are found in the backlimb (varying from 3.4 – 13.2%), in the hinge zone (2.3 – 10.9%), and in the forelimb of the fold (2.2 – 6.3%) (Fig. 6c). Permeabilities vary in the backlimb (0.005 – 5.7 mD), in the hinge zone (0.02 – 26.4 mD), and in the forelimb of the fold (0.02 – 0.6 mD) (Fig. 6c).

In the Kurra Chine Formation, porosities ranging from 9.5 – 18.9% are found in the backlimb of the Gara Anticline, 6.1% in the hinge zone, and 2.7 – 12.8% in the forelimb of the fold (Fig. 6d). Similarly, variable permeabilities are found in the backlimb (0.1 – 16.5 mD), in the hinge zone (0.04 mD), and in the forelimb of the fold (0.0003 – 0.7 mD) (Fig. 6d).

6. Ora Anticline

The Ora Anticline is located 50 km NE of Duhok City (Figs. 1a, b). Despite its location within the Imbricated Zone, its outcrops provide the type section of the Kurra Chine Formation. The Ora Anticline is an E-W trending asymmetrical anticline which verges

towards south. It is a hanging wall anticline with a steep forelimb that is carried on a south-directed thrust (Figs. 7a, b). Parasitic folds verging towards the south are also observed in the lower part of the Kurra Chine section. The structure is traceable along its length for 25 km and has a width of 11 km. The Khabour Quartzite Formation (Ordovician) makes up the core of the anticline, whereas other Palaeozoic and Mesozoic units crop out along its flanks (Figs. 7a, b). Both dextral and sinistral strike-slip faults have been observed in the southern limb of the Ora Anticline (Fig. 7a).

The Kurra Chine Formation crops out along the northern and southern limbs of the Ora Anticline. Due to security considerations, it was only possible to collect fracture data and samples from the southern limb of the fold. The fracture data were collected from three localities at different stratigraphical levels on this southern limb. The unit comprises bedded limestone in the lower part, massive dolomitised limestone in the middle part, and karstified dolomitised limestone in its upper part. The upper part of the Kurra Chine Formation is highly deformed and structurally brecciated.

6.1. Fracture orientation and intensity in the Ora Anticline

As noted above, fracture datasets were collected at three localities on the southern forelimb of the Ora Anticline (Figs. 7a, b). Most fractures dip sub-perpendicular to bedding and may therefore be categorised according to trend. Four fracture sets trending N-S, E-W, NE-SW and NW-SE were identified from the stereograms (Fig. 7a). Most fractures are veins filled with calcite. The N-S and NE-SW fracture sets at locality KC-2 together form a conjugate set, with the acute bisector forming parallel to a local NNE-SSW trending sinistral strike slip fault (Fig. 7a). The three locations are however in close proximity to a strike-slip fault and lie within the damage zone of the fault. 1D fracture density (P10) ranges between 0.46 and 2.89

m^{-1} for all fracture sets. In terms of their length, fractures are observed to be short (0.25 – 3 m) at locality KC-1, are relatively longer (4 – 15 m) at locality KC-2, while their lengths are obscured by scree at locality KC-3. Furthermore, the majority of fracture terminations are of fracture-abutting type at all three localities.

6.2. Petrophysical properties in the Ora Anticline

The Kurra Chine Formation exposed in the Ora Anticline displays a general trend of increasing permeability with increasing porosity (Fig. 6b). The porosities range over two orders of magnitude (0.8 - 19.2%), while permeabilities vary over four orders of magnitude (0.0015 – 19.8 mD) (Fig. 6b). The Kurra Chine datasets come from the steep forelimb of the Ora Anticline and damage zones of strike-slip faults. The high porosities and high permeabilities can be attributed to the structural position of the fold and fault zones, and presumably related to micro fractures observed in the core plugs.

7. Ranya Anticline

The Ranya Anticline is located in the Highly Folded Zone of the Zagros fold and thrust belt about 75 km east of Erbil City (Figs. 1a, b). It is an asymmetrical anticline with NE-directed vergence and a NW-SE orientated fold axis (Figs. 8a, b). The anticline extends for 27 km and is 7 km wide (Fig. 1b). The Sehkaniyan Formation is exposed at the core of the anticline, which has been extensively eroded resulting in a deep valley along the fold axis.

7.1. Fracture orientation and intensity in the Ranya Anticline

Fracture data and samples were collected near Hanjira village, which is located a few kilometres to the north of Ranya City (Fig. 8a). The study area is located within the forelimb of the Ranya Anticline, which comprises Sehkaniyan and Sarki formations (Lower Jurassic) (Figs. 8a, b). The datasets have been collected from the better exposed upper part of the Sehkaniyan Formation (Fig. 8b).

The fracture data in the Sehkaniyan Formation shows a dominant N-S orientation, a less dominant hinge parallel trend represented by NW-SE fractures, and a hinge perpendicular trend represented by NE-SW orientations (Fig. 8a). In the overlying Sargelu Formation, fracture orientations at locality SG-1 are defined by two dominant orthogonal sets of NNE-SSW and WNW-ESE fractures (Fig. 8a). Most fractures are sub-perpendicular to bedding. Fractures in the Sargelu Formation are confined by thin limestone layers. Furthermore, fractures in the limestones of the Sargelu Formation are generally more abundant and display a greater fracture density than those in the massive dolostones and dolomitised limestones of the Sehkaniyan Formation. The average 1D fracture density (P10) in the Sehkaniyan Formation is 1.47 m^{-1} while it is 5.27 m^{-1} in the overlying Sargelu Formation (Fig. 9). Most of these fractures belong to the ~N-S striking fracture set. The fracture lengths are variable and range from 0.25 m to up to more than 7 m, where fracture tips are obscured. Fracture terminations are of fracture-abutting type. Furthermore, most fractures are joints at locality SK-2, whereas they are veins filled with calcite at localities SK-1 and SK-3 as well as locality SG-1.

7.2. Petrophysical properties in the Ranya Anticline

The Sehkaniyan Formation in the Ranya Anticline displays a general trend of increasing permeability with increasing porosity (Fig. 6a). The porosities are distributed within one order of magnitude (1.1 – 7.5%), while permeabilities are spread over three orders of magnitude (0.001 – 1.5 mD) (Fig. 6a). The Sehkaniyan dataset was sampled from the forelimb of the Ranya Anticline, and shows a similar distribution to those measured in the forelimb of the Gara Anticline (Fig. 6c). Furthermore, the porosity-permeability datasets from the Sehkaniyan outcrops make a clustering pattern around a best-fit line (Fig. 6a), whereas the porosity-permeability trend in the Kurra Chine Formation has a scattering pattern around a best-fit line (Fig. 6b).

7.3. Permeability versus confining pressure

In order to investigate the impact of burial depth on permeability reduction and fluid flow within the Kurra Chine and Sehkaniyan formations, five samples from each rock unit are analysed for permeability using stepwise increasing hydrostatic confining pressure (Figs. 10a, b). The data were collected from 20 MPa up to a maximum confining pressure of 100 MPa. The Kurra Chine reservoir can be represented by a confining pressure of 60 MPa, which corresponds to approximately 3 km of burial depth. Permeability values show their most significant reduction over the first 20 MPa of applied confining pressure (Fig. 10b). Ratios between initial and final permeability values range from 0.27 to 0.09 in the Kurra Chine and from 0.46 to 0.17 in the Sehkaniyan (Figs. 10a, b). The datasets show a variation in confining pressure permeability of the Kurra Chine and Sehkaniyan. The permeabilities of the Kurra Chine Formation show variation of one order of magnitude (0.02-0.62 mD) at a confining pressure of 60 MPa. The permeabilities of the Sehkaniyan Formation range within one order

of magnitude (0.11-0.73 mD) at a confining pressure of 60 MPa (Figs. 10a, b). At high confining pressure, permeability decreases dramatically implying pore, crack or pore throat closure, while at low confining pressure, the permeability increases slightly, perhaps due to dilatant opening of voids (cracks, pores or pore throats).

8. Shaikhan Anticline

The Shaikhan Anticline is located about 85 km to the northwest of Erbil City and is a double-plunging fold within the Highly Folded Zone of the Zagros fold and thrust belt (Figs. 1a, b). The Shaikhan Anticline is an E-W trending asymmetrical anticline which verges towards north, is 30 km long and 7 km in width (Figs. 11a, b). Eight hydrocarbon reservoir formations of Cretaceous and Triassic ages were encountered in the SH-1B well, among them are the Alan, Mus (Sehkaniyan equivalent) and Kurra Chine formations (Figs. 2, 11b).

8.1. Fracture orientation and intensity in the Shaikhan Anticline

Wells are located around the Shaikhan Anticline including the crest (SH-1), the backlimb (SH-2), and the forelimb close to the western nose of the fold (SH-4) (Fig. 11a). Three types of fractures were interpreted from FMI and XRMI image logs: conductive (open), resistive (mineralised) and hybrid (part-open, part-mineralised), as well as faults. The interpreted fractures (mainly conductive and hybrid) and faults show a dominant N-S orientation in the Sehkaniyan Formation in wells SH-1 and SH-2, and a dominant WNW-ESE striking fractures (mainly resistive) in the Kurra Chine Formation in well SH-4 (Fig. 11a). The WNW-ESE fractures were observed in the damage zones of WNW-ESE striking faults. The fault orientations in well SH-4 parallel the fold axis, and also align with the E-W oriented main thrust that cuts through the forelimb of the Shaikhan Anticline. The average corrected fracture

intensity (P10_C) of the Mus-Adaiyah, Alan (Sehkaniyan equivalent) and Kurra Chine formations in wells SH-1, SH-2 and SH-4 are 0.3 m^{-1}, 0.75 m^{-1} and 0.74 m^{-1}, respectively. Furthermore, the fracture density is higher within stratigraphical levels associated with limestones, where two cross-cutting fracture sets exist in some cases.

8.2. Petrophysical properties in the Shaikhan Anticline

There is a general trend of decreasing porosity with increasing P-wave acoustic velocity in the Sehkaniyan and Kurra Chine intervals in the Shaikhan wells (Figs. 12a, b). The Sehkaniyan Formation displays a clustered trend of decreasing porosity with increasing acoustic velocity (Fig. 12a). The Kurra Chine Formation shows a considerable scattering in P-wave velocity (Fig. 12b). Furthermore, the Sehkaniyan Formation shows higher velocity for a given porosity at the subsurface than outcrops (Figs. 12a, 13a). The petrophysical properties vary with lithology at different stratigraphical levels. For example, the best reservoir quality is found at a stratigraphic level which comprises a vuggy dolomite facies in both units (Figs. 12a, b).

9. Swara Tika Anticline

The Swara Tika Anticline is a well-defined double-plunging fold located 10 kilometres to the SW of the Gara Anticline (Figs. 1a, b). The fold axis is oriented WNW-ESE within the Highly Folded Zone of the Zagros fold and thrust belt (Fig. 11a). The Swara Tika Anticline is an asymmetrical fold which verges towards south, is 15 km along the fold axis and 3 km in width (Figs. 11a, b). The bedding dip from core data is around 10º, reflecting the position of the wells close to the crest of the anticline. The core data does not show much evidence for layer-parallel slip, once again reflecting the location of the cores from wells drilled at the crest of the anticline. Bedding-parallel cleavage is however observed from core data, and typically

displays a dextral sense of movement. The primary reservoir units are the Cretaceous Qamchuqa, Jurassic Sehkaniyan and the Triassic Kurra Chine dolomite reservoirs.

9.1. Fracture orientation and intensity in the Swara Tika Anticline

The fractures and faults interpreted from FMI and XRMI image logs show dominant N-S trends in well ST-1 and dominant NNE-SSW trend in well ST-2, and a less abundant NW-SE fault and fracture set (Fig. 11a). Conductive (open) and hybrid (part-open, part-mineralised) fractures are abundant in well ST-1 whereas hybrid fractures are dominant in well ST-2. Fractures of Jurassic intervals from the Swara Tika cores are partially filled with calcite veins and invaded with oil. Many fractures in Jurassic and Triassic intervals are partially mineralised by calcite, leading to a reduction in fracture porosity. The average fracture aperture was calculated in well ST-2 using the equation introduced by Luthi and Souhaite (1990). This method depends on the fracture width and mud filtrate resistivity. However, fracture aperture measurement is also dependent on other factors such as mud weights, while drilling may influence the amount of invasion, and minor changes in lithology which also affect the resistivity values. The measured fracture porosity ranges between 0.01% and 0.06% in the Sehkaniyan Formation in well ST-2. High fracture porosity corresponds to high aperture and fracture density. High fracture density may indicate a fracture corridor, or can be a function of lithological-mechanical control. The average corrected fracture intensity (P10_C) of the Alan-Mus-Adaiyah (Sehkaniyan equivalent) and Alan Formation in wells ST-1 and ST-2 are 0.33 m^{-2} and 0.31 m^{-3}, respectively.

9.2. Petrophysical properties in the Swara Tika Field

There is a general trend of decreasing porosity with increasing P-wave velocity in the Sehkaniyan and Kurra Chine intervals in the Swara Tika wells (Figs. 12c, d). Similar to the Shaikhan datasets, the Sehkaniyan Formation shows higher acoustic velocity for a given porosity at the subsurface when compared to the outcrops (Figs. 12c, 13a), while the Kurra Chine Formation displays a significant scattering in acoustic velocity (Fig. 12d).

10. Reservoir characteristics of the Kurra Chine and Sehkaniyan formations

The Kurra Chine and Sehkaniyan formations are important fractured carbonate units in the Upper Triassic and Lower Jurassic plays in Iraqi Kurdistan. In almost all recent wells that have been drilled and encountered these units in the region, they exhibit hydrocarbon show. Their lithologies are heterogeneous and therefore studying their fracture patterns and petrophysical properties can help to understand reservoir types.

10.1. Petrophysical properties

Despite low matrix porosity and permeability in both the Kurra Chine and Sehkaniyan formations, they work as reservoirs because of the fractures. Both units can be considered as reservoir type II as fractures provide the essential reservoir permeability, with low matrix contribution (Nelson, 2001). In the current study, porosities of the Sehkaniyan Formation vary between 1% and 14% at outcrops and subsurface, and permeabilities show a range of four orders of magnitude (0.001-26 mD) (Fig. 6a). Porosities of the Kurra Chine Formation range from 0.8% to about 19% at outcrops and subsurface, and permeabilities show higher variation

(about five orders of magnitude, 0.0003-20 mD) (Fig. 6b). Overall there is a general trend of increasing permeability with increasing porosity. Even at low poro-perm, the limestone and dolomite data show the typical pattern of dolomites having higher permeability for a given porosity than limestones, maybe because of well-connected intercrystalline pores (Figs. 6a, b), or may be because of dilation of micro-fractures due to overburden removal at surface. In comparison, there is lower porosity and permeability in the Sehkaniyan Formation than in the Kurra Chine. In addition there is a scattering of the Kurra Chine data at high porosity and permeability, whereas the Sehkaniyan shows clustering (Figs. 6a, b).

The structural position on regional folds may control the distribution of porosity and permeability of the Sehkaniyan and Kurra Chine rocks. For example, the same stratigraphic levels display higher porosities and permeabilities on the backlimb of the Gara Anticline when compared to the forelimb (Figs. 6c, d). It is observed that positon on the fold also controls spatial distribution of fracture patterns in the Sehkaniyan and Kurra Chine formations.

There is a general trend of decreasing porosity with increasing P-wave acoustic velocity (Figs. 12, 13). The velocity-porosity data show similar trends to the Kurra Chine Formation at outcrops and subsurface. However, the trend is steeper (lower velocity for a given porosity) for the Sehkaniyan Formation at outcrops than in the subsurface (Figs. 12a, c, 13a). This variation in slope between outcrop and subsurface data can be attributed to the saturated rock densities with fluids (hydrocarbon and/or water) at subsurface. The Kurra Chine Formation shows scattering in acoustic velocity, while the Sehkaniyan shows clustering (Figs. 13a, b). Furthermore, the structural position on the fold controls the distribution of porosity and P-wave velocity. For example, the highest velocities correspond to the forelimbs of the anticlines (Fig. 13c). In addition, the Sehkaniyan porosity-permeability datasets from outcrops make a clustering pattern around a best-fit line (Fig. 6a), whereas the porosity-

permeability data from the Kurra Chine Formation has a scattering pattern around a best-fit line (Fig. 6b).

10.2. Elastic properties

We perform this analysis to compare elastic properties of surface rocks with those from the subsurface. The Voigt upper bound and Reuss lower bound on the elastic moduli of rocks provide a useful basis for porosity-velocity relations (Avseth et al., 2005). The bounds are valuable rock physics tools since well logs give information on constituents and their volume fraction, but relatively little about grain and pore microstructure (Avseth et al., 2005). A simple mixture of two constituents such as two different minerals, or a mineral plus fluid (water, oil or gas), can be used. At any given volume fraction of constituents, the effective modulus of the mixture will fall between the bounds, depending on the geometric details. It is observed that with increasing diagenesis, the rock properties lie along steep trends that extend upwards from the Reuss bound toward the mineral end point at zero porosity (Avseth et al., 2005).

In the current study, a mixture of calcite and brine is used for the Sehkaniyan Formation, and a mixture of calcite, dolomite and brine for the Kurra Chine Formation. The brine is used as the second constituent for the fluid saturated well data. Despite the homogenous stratigraphic interval of the Kurra Chine Formation in well ST-1, a significant scattering and enhancement of porosities are observed in dolomites (Fig. 12d). The logged stratigraphy is constrained from mud logging and cutting data rather than on the basis of detailed micro-scale lithofacies analysis. Therefore, this scattering and enhancement of porosities are interpreted to be a result of the intercrystalline pores that formed by diagenetic processes. Another possibility for the increased scattering and enhanced porosity in the Kurra

Chine Formation in well ST-1 compared to well SH-1 relates to the Kurra Chine consisting of massive dolomites in well ST-1, whereas it comprises a mixture of limestones, dolomites and evaporites in well SH-1.

11. Discussion

11.1. Comparison of outcrop and subsurface fracture data

Fractures observed and sampled in the Gara outcrops show layer parallel shearing such as those at localities SK-1 and SK-2 (Fig. 5a). However, the core data do not display much evidence for layer-parallel slip because the cores come from a well that drilled on the crest of the Swara Tika Anticline. Bedding-parallel cleavage is however observed from core data, and typically displays a dextral sense of movement. Calcite veins are observed to be folded in Swara Tika cores, indicating they are fold-related and bending is earlier or at least synchronous with folding. Hence, flexural slip folding is the possible mechanism of folding which is characterised by bedding-parallel slip striation and bending (Reif et al., 2012). Tectonic stylolites were observed within the Kurra Chine Formation in the Gara Anticline. This stratigraphic unit is probably below the neutral surface of the fold and could therefore help support the flexural slip folding mechanism.

Fracture orientations show a clear relationship to the local fold axis in both the outcrops and subsurface (e.g. Gara, Shaikhan, Swara Tika). In particular, a fracture set parallels the WNW-ESE fold axis and a NNE-SSW fracture set is oriented perpendicular to the fold axis. However, some fractures do not show any relation to the local folding. These fractures may be formed pre-folding, post-folding, or could be interpreted as interference of two different shortening phases, related to folding (Csontos et al., 2012). Some fracture orientations display symmetry relative to the local strike slip fault in the Ora Anticline (Fig.

7a). This fault could primarily control the overprinted NE-SW fractures, while the position on the fold controls the fold-related N-S fractures. Other fracture orientations exhibit a symmetrical relation to the maximum horizontal stress direction such as in the Ranya Anticline (Fig. 8a). The present *in-situ* maximum horizontal tectonic stress direction in Kurdistan is oriented ~NNE-SSW, based on regional geology and the world stress data (Heidbach et al., 2008). Furthermore, local rotations (10º-15º) of fracture orientations were observed and are attributed either to curvature in the fold axis or fault movement (Csontos et al., 2012).

There is likely lithological and/or bed thickness control on fracture density such as in the Ranya Anticline, where 1D fracture density (P10) is over three times higher in the Sargelu thin-bedded limestones than the underlying Sehkaniyan massive dolomites (Fig. 9). Fractures are generally more linear, smoother and evenly distributed in limestones compared to dolomites.

In the Gara Anticline, the NNE-SSW fractures are oriented parallel to the maximum horizontal principal stress direction and perpendicular to the fold axis. Hinge parallel fractures may have formed due to local outer arc extension of the folds. Open fractures are observed to strike perpendicular to the fold axis in the Gara Anticline. Hinge normal fractures may be created as a pericline grows along the length of its axis, with bed dips initially increasing around the plunging nose, before being rotated and reducing as the rocks then form part of the general hinge. i.e. the nose of the fold has migrated along strike into new rocks. Bitumen staining along the fractures and vugs is often found along thrust faults in the Sehkaniyan and Kurra Chine formations. For example, the bitumen filled-fractures in the Kurra Chine Formation in the Gara Anticline are oriented perpendicular to the compressional direction and the fold axis, whereas bituminous fractures in the Sehkaniyan Formation are oriented parallel to the thrust faults and fold axis. As mentioned above, the observed open fractures are striking

perpendicular to the fold axis in the Gara Anticline. These fractures are partially cemented with calcite, while the innermost part is filled by bitumen. This could mean that bitumen invaded after the fracturing process, suggesting that hydrocarbon migration is young and possibly postdates folding (Csontos et al., 2012). It could also be interpreted that the fluid used to reach failure was hydrocarbon or a hydrocarbon/water emulsion and as such is coincident with the fracture development and not independent. Fractures require both critical stress and continuous elevated pore pressure to form (see Cosgrove, 2015; MacKay, 2015) and as such the fracture become temporary fluid conduits. This may suggest that emplacement of hydrocarbons and fold development occur simultaneously. These fractures with bitumen inclusion are mostly observed within damage zones of thrust faults.

Both the Shaikhan and Swara Tika fields are dominated by the N–S fracture set (hinge-perpendicular) whereas the E–W fracture set (hinge-parallel) is not present. The absence of the E-W fracture set may be attributed to (i) the orientation of the *in-situ* stress, which has a tendency to keep the N-S fractures open thereby providing a sufficient contrast to be resolved on the borehole image logs. Correspondingly, hinge-parallel E-W fractures would be suppressed (Awdal et al., 2013); and/or (ii) a low compressional stress within the reservoirs could also partly explain the relatively open state of the N-S fracture system (Garland et al., 2010). Furthermore, stress release during uplift is likely to enhance the differences in fracture pattern between the surface and subsurface anticlines.

11.2. Comparison of outcrop and subsurface petrophysical data

The petrophysical properties of the Kurra Chine Formation show a similar trend in the outcrop dry samples and subsurface fluid saturated datasets. Most dolomites have higher average porosities and permeabilities than limestones. In the literature, it is documented that a

slight increase in porosity develops in the early stages of dolomitisation of limestones, but a sudden increase occurs with greater amounts of dolomitisation (e.g. Flügel, 2010). The Kurra Chine limestone and dolomite data therefore show the typical pattern of dolomites having higher permeability for a given porosity than limestones, presumably because of well-connected intercrystalline pores. On the other hand, limestones of the Sehkaniyan Formation show lower porosities, and may be due to low matrix porosity with no secondary porosity developed in limestones. Furthermore, the velocity-porosity trend is steeper (lower acoustic velocity for a given porosity) in the Sehkaniyan outcrop dry sample measurements than its fluid saturated subsurface measurements. The variation in slope between outcrop and subsurface may be related to the saturated rock densities with fluids (hydrocarbon and/or water) at subsurface.

The matrix porosity and permeability of the Kurra Chine and Sehkaniyan formations depends on the lithology, structural position on the fold, proximity to the local faults, and other factors that have not been discussed in this paper such as gas expansion, scale of lithologic heterogeneity, grain size, pore type, extent of porosity enhancing diagenesis and cement dissolution. The porosity and permeability values range over 2 – 5 orders of magnitude due to the different lithologies of the Kurra Chine and Sehkaniyan formations. Dolomites generally have better permeability of effective porosity than limestones and is perhaps due to interconnected pores. Vuggy porosity facies were found in the damage zones of thrust faults. In terms of structural position, the hinge and backlimb seem to have better porosities and permeabilities than the forelimb of the Gara Anticline (Figs. 6c, d). This may be due to the presence of vuggy and interconnected porosity of dolomite facies, or may be due to the existence of natural micro-fractures in the core plug samples that offer additional porosity. Likely the fractures add significantly to the permeability of the system and as such the permeability sampled by the core plugs will under-estimate the permeability of the system

as a whole. The relationship between micro-fractures and fractures observed and sampled in the outcrops are not studied in this paper.

11.3. Implications for reservoir connectivity and production

Both the Kurra Chine and Sehkaniyan formations are potential fractured reservoirs in several oil and gas fields in Kurdistan. Despite their low matrix porosity and permeability, the Kurra Chine and Sehkaniyan formation are extensively fractured and have a good fracture network. Both units can be considered as reservoir type II as fractures provide the essential reservoir permeability, with less matrix contribution (Nelson, 2001). The prediction of the permeability and connectivity is challenging, as indicated by initial high flow rates from discoveries followed by a dramatic drop off during production.

The fracture interpretation of borehole images from the Shaikhan and Swara Tika fields shows that the most dominant orientation of conductive (open) and hybrid (part-open part-mineralised) fractures is N-S in wells SH-1, SH-2, ST-1 and ST-2. The dominant N-S conductive and hybrid fractures were interpreted within the Alan, Mus and Adaiyah (Sehkaniyan equivalent) formations. However, a dominant resistive (mineralised) fracture strike orientation of WNW-ESE was interpreted in well SH-4 within the Kurra Chine Formation. The variation in fracture strike orientation of well SH-4 compared to other wells may be due to the occurrence of WNW-ESE striking faults. The WNW-ESE striking mineralised fractures were interpreted within damage zones of the WNW-ESE striking faults. Hence, these faults may primarily control the overprinted WNW-ESE fractures while the position on the fold could control the fold-related N-S fractures. In terms of geometry, the dominant N-S open and part-open fracture strike orientation is perpendicular to the fold axes, which indicates anisotropic permeability with the maximum fracture permeability aligning in

the N-S direction. In terms of drilling dynamics, the total mud losses and hydrocarbon shows at reservoir intervals confirm the presence of various scales of conductive fractures and faults.

11.4. Conceptual fracture model

Based on the current datasets, a conceptual model is proposed for fractures in the studied thrust-related anticlines (Fig. 14). The proposed conceptual model describes the various components of the fracture network in terms of geometry and dynamic behaviour. Three stages of fracturing are suggested in the studied anticlines (Fig. 14). This conceptual model is based on actual fracture results in this study and also supported by earlier studies carried out in the Zagros fold and thrust belt in Iraqi Kurdistan (e.g. Csontos et al., 2012; Reif et al., 2012; Awdal et al., 2013). A pre-folding stage of hinge-perpendicular fractures is proposed to have been formed by the far-field stress during the collision between the Arabian and Eurasian plates in a foreland position (Ahmadhadi et al., 2008). Similar fracturing has been suggested elsewhere in the Zagros (e.g. Casini et al., 2011; Tavani et al., 2011; Awdal et al., 2013). An early-folding stage of hinge-parallel fractures and faults are possibly formed due to outer arc extension in the folds, and could be associated with layer-parallel and intra-layer shear. The oblique fractures in the forelimb are suggested to post-date the hinge-parallel and hinge-perpendicular fracture sets. These oblique fractures are proposed to be related to reactivation of, and stress reorientation around, basement faults, as suggested elsewhere along the Zagros fold and thrust belt (e.g. Fard et al., 2006; Stephenson et al., 2007; Ahmadhadi et al., 2008; Tavani et al., 2011). Alternatively, they could be caused by nearly bedding-perpendicular shortening and lateral extension during significant flexing in the forelimb. The latter interpretation fits best with the dominant position in the steeper dipping forelimb in conjunction with the proposed late development of the conjugate oblique fracture sets. Furthermore, mechanical anisotropy cause some fracture formation. Bedding-perpendicular

fractures could be formed by the mechanical anisotropy created by bedding and it is not necessarily related to early (pre-folding) fracture set.

12. Summary and conclusions

Based on a comparison of outcrop fracture data, subsurface data from wireline and image logs and laboratory petrophysical measurements, the following conclusions can be drawn.

- The current study focuses on the potential control that folds may exert on the fracture patterns and petrophysical properties of fractured carbonates.
- Fracture sets may show relationships to local folding in the study area. Fractures may form a hinge-parallel set, a hinge-perpendicular set and two conjugate oblique sets whose acute angle bisects the shortening direction. In addition, some fractures show a relationship with the present day *in-situ* maximum horizontal stress direction or local strike-slip faulting.
- N-S dominant open and part-open fracture orientation is perpendicular to the Shaikhan and Swara Tika fold axes, which may indicates anisotropic permeability with the maximum fracture permeability aligning in the N-S direction.
- Fracture intensity may be influenced by lithology and/or bed thickness in the study area. Fracture intensity is markedly higher in the Sargelu thin-bedded limestones than the underlying massive Sehkaniyan Formation, and the Sehkaniyan may be influenced by dolomitisation.
- Three stages of fracturing are proposed: a pre-folding stage of hinge-perpendicular fractures, an early-folding stage of hinge-parallel fractures and faults, and a post-dating stage of oblique fractures.
- Petrophysical properties in the Kurra Chine and Sehkaniyan formations may be controlled by lithology, position on folds and spatial distribution within faults.

- Some differences between surface and subsurface fracture patterns can be explained by stress release during uplift or exhumation, diagenesis and differences in mechanical behaviour.
- Understanding fracture patterns can help to make better predictions of fluid flow in subsurface reservoirs. Therefore, the results of this study may have implications for reservoir connectivity and fracture modelling.

Acknowledgements

The authors thank the Ministry of Natural Resources in Iraqi Kurdistan Region for permission to publish this paper. Gulf Keystone Petroleum Ltd. and HKN Energy Ltd. are acknowledged for providing the subsurface datasets. Great thanks to Colin Taylor at the University of Aberdeen for his assistance in the laboratory work. Thoughtful reviews by two anonymous referees improved the clarity of the paper. Graham Banks is thanked for his helpful and constructive review on a late version of the manuscript, which has significantly improved this paper.

References

Agosta, F., 2008. Fluid flow properties of basin-bounding normal faults in platform carbonates, Fucino Basin, central Italy. In: Wibberley, C.A.J., Kurz, W., Imber, J., Holdsworth, R.E., Collettini, C. (eds.) The Internal Structure of Fault Zones: Implications for Mechanical and Fluid-Flow Properties. 299, 277–291.

Ahmadhadi, F., Daniel, J.-M., Azzizadeh, M., Lacombe, O., 2008. Evidence for pre-folding vein development in the Oligo-Miocene Asmari Formation in the Central Zagros Fold Belt, Iran. Tectonics, 27, TC1016.

Aliverti, E., Biron, M., Francesconi, A., Mattiello, D., Nardon, S., Peduzzi, C. 2003. Data Anlaysis, processing and 3D fracture network simulation at wellbore scale for fractured reservoir description. In: Ameen, M.S. (ed.) Fracture and In-Situ Stress Characterization of Hydrocarbon Reservoirs. Geological Society, London, Special Publications, 209, 27–37.

Al-Breefkani, M.J.N., 2008. Structural and tectonic analysis of Northern Thrust Zone, east Khabour river, Northern Iraq. PhD thesis. Unpublished. University of Mosul.

Ameen, M.S., Buhidma, I.M., Rahim, Z., 2010. The function of fractures and in-situ stresses in the Khuff reservoir performance, onshore fields, Saudi Arabia. AAPG Bulletin 94, 27–60.

Antonellini, M., Mollema, P.N., 2000. A Natural Analog for a Fractured and Faulted Reservoir in Dolomite: Triassic Sella Group, Northern Italy. AAPG Bulletin 84, 314–344.

Aqrawi, A.A.M., Goff, J.C., Horbury, A.D., Sadooni, F.N., 2010. The Petroleum Geology of Iraq. Scientific Press, Beaconsfield. 424.

Avseth, P., Mukerji, T., Mavko, G., 2005. Quantitative Seismic Interpretation, Applying Rock Physics Tools to Reduce Interpretation Risk. Cambridge University Press, Cambridge, 355.

Awdal, A.H., Braathen, A., Wennberg, O.P., Sherwani, G.H., 2013. The characteristics of fracture networks in the Shiranish formation of the Bina Bawi Anticline; comparison with the Taq Taq Field, Zagros, Kurdistan, NE Iraq. Petroleum Geoscience 19, 139–155.

Aydin, A., 2000. Fractures, faults, and hydrocarbon entrapment, migration and flow. Marine and Petroleum Geology 17, 797–814.

Banks, G., 2013. Anatomy of the foreland section of the Zagros Orogenic Wedge: Implications for hydrocarbon trap geometries. In: Hydrocarbon exploration in the Zagros Mountains of Iraqi Kurdistan and Iran. The Geological Society, London.

Barr, D., Savory, K.E., Fowler, S.R., Arman, K., Mcgarrity, J.P., 2007. Pre-development fracture modelling in the Claire field, west of Shetland. Geological Society Special Publication 270, 205-225.

Bellahsen, N., Fiore, P., Pollard, D.D., 2006. The role of fractures in the structural interpretation of Sheep Mountain Anticline, Wyoming. Journal of Structural Geology, 28, 850–867.

Bergbauer, S., 2007. Testing the predictive capability of curvature analysis. In: Jolley, S.J., Barr, D., Walsh, J.J., Knipe, R.J. (eds) Structurally Complex Reservoirs. Geological Society, London, Special Publications, 292, 185–202.

Bergbauer, S., Pollard, D.D., 2004. A new conceptual fold-fracture model including prefolding joints, based on the Emigrant Gap anticline, Wyoming. GSA Bulletin, 116, 294-307.

Bourne, S.J., Brauckmann, F., Rijkels, L., Stephenson, B.J., Weber, A., Willemse, E.J.M., 2000. Predictive modelling of naturally fractured reservoirs using geomechanics and flow simulation. Paper ADIPEC 0911 presented at the 9th Abu Dhabi International Petroleum Exhibition and Conference, Abu Dhabi, U.A.E., 10.

Buday, T., 1980. The Regional geology of Iraq. Vol.1: Stratigraphy and Palaergeography. Publications of GEOSURV, Baghdad, 445.

Casini, G., Gillespie, P.A., Vergés, J., Romaire, I., Fernández, N., Casciello, E., Saura, E., Mehl, C., Homke, S., Embry, J.-C., Aghajari, L., Hunt, D.W.. 2011. Sub-seismic fractures in foreland fold and thrust belts: Insight from the Lurestan Province, Zagros Mountains, Iran. Petroleum Geoscience, 17, 263–282.

Cooper, M., 2007. Structural style and hydrocarbon prospectivity in fold and thrust belts: A global review. Geological Society Special Publication 272, 447–472.

Cosgrove, J.W., 2015. The association of folds and fractures and the link between folding, fracturing and fluid flow during the evolution of a fold–thrust belt: a brief review. In: Richards, F.L., Richardson, N.J., Rippington, S.J., Wilson, R.W., Bond, C.E. (eds) Industrial Structural Geology: Principles, Techniques and Integration. Geological Society, London, Special Publication, 421.

Csontos, L., Sasvári, Á., Pocsai, T., Kósa, L., Salae, A.T., Ali, A., 2012. Structural evolution of the northwestern Zagros, Kurdistan Region, Iraq: Implications on oil migration. GeoArabia 17, 81–116.

Dershowitz, W., Herda, H.H. 1992. Interpretation of fracture spacing and intensity. Proceedings of the 33rd US Symposium on Rock Mechanics, Santa Fe, NM, 757.

de Verteuil, N., Flannery, J., Granath, J., Odell, V., Richardson, R., Studlick, J., Wawrzyniec, T., 2011. Overview of the geology of Kurdistan. Dynamic Global Advisors.

Fard, I.A., Braathen, A., Mokhtari, M., Alavi, S.A. 2006. Interaction of the Zagros Fold–Thrust Belt and the Arabian-type, deep-seated folds in the Abadan Plain and the Dezful Embayment, SW Iran. Petroleum Geoscience, 12, 347–362.

Flügel, E., 2010. Microfacies of Carbonate Rocks, Analysis, Interpretation and Application. Second Edition, Springer. 984.

Fossen, H., 2010. Structural Geology. Cambridge University Press, Cambridge. 463.

Garland, C.R., Abalioglu, I., Akca, L., Cassidy, A., Chiffoleau, Y., Godail, L., Grace, M.A.S., Kader, H.J., Khalek, F., Legarre, H., Nazhat, H.B., Sallier, B.. 2010. Appraisal and

development of the Taq Taq field, Kurdistan region, Iraq. In: Vining, B.A., Pickering, S.C. (eds) Petroleum Geology: From Mature Basins to New Frontiers – Proceedings of the 7th Petroleum Geology Conference. Geological Society, London, 7, 801–810.

Granath, J.W., Odell, V.H., 2014. Structural architecture of the NW Kurdistan thrust belt: elements of the 'Dohuk passive roof'. AAPG International Conference and Exhibition, Istanbul.

Healy, D., Neilson, J.E., Haines, T.J., Michie, E.A., Timms, N.E., Wilson, M.E., 2015. An investigation of porosity–velocity relationships in faulted carbonates using outcrop analogues. Geological Society, London, Special Publications, 406, 261-280.

Heidbach, O., Tingay, M., Barth, A., Reinecker, J., Kurfeß, D., Müller, B., 2008. The World Stress Map database release 2008, doi:10.1594/GFZ.WSM.Rel2008.

Homke, S., Vergés, J., Garcés, M., Emami, H., Karpuz, R. 2004. Magnetostratigraphy of Miocene–Pliocene Zagros foreland deposits in the front of the Push-e Kush Arc (Lurestan Province, Iran). Earth and Planetary Science Letters, 225, 397–410.

Homke, S., Vergés, J., Serra-Kiel, J., Bernaola, G., Sharp, I., Garcés, M., Montero-Verdú, I., Karpuz, R., Goodarzi, M.H., 2009. Late Cretaceous–Paleocene formation of the proto–Zagros foreland basin, Lurestan Province, SW Iran. GSA Bulletin, 121, 963–978.

Huang, Q., Angelier, J. 1989. Fracture spacing and its relation to bed thickness. Geological Magazine, 126, 355–362.

Jassim, S.Z., Goff, J.C., 2006. The Geology of Iraq. Dolin, Prague. 341.

Kubli, T.E., McKenna, S., 2013. Deformation history and thin-skinned vs. thick-skinned tectonics in the Zagros fold and thrust belt of Southern Kurdistan. In: Hydrocarbon

exploration in the Zagros Mountains of Iraqi Kurdistan and Iran. The Geological Society, London.

Lacombe, O., Bellahsen, N., Mouthereau, F. 2011. Fracture patterns in the Zagros Simply Folded Belt (Fars, Iran): Constraints on early collisional tectonic history and role of basement faults. Geological Magazine, 148, 940–963.

Lapponi, F., Casini, G., Sharp, I., Blendinger, W., Fernández, N., Romaire, I., Hunt, D., 2011. From outcrop to 3D modelling: a case study of a dolomitized carbonate reservoir, Zagros Mountains, Iran. Petroleum Geoscience, 17, 283–307.

Luthi, S.M., Souhaite, P., 1990. Fracture apertures from electrical borehole scans. Geophysics 55, 821–833.

Lønøy, A., 2006. Making sense of carbonate pore systems. AAPG Bulletin, 90, 1381–1405.

MacKay, P., 2015. The role of fluid pressure in contractional systems: examples from the Southern Canadian Rocky Mountains. In: Richards, F.L., Richardson, N.J., Rippington, S.J., Wilson, R.W., Bond, C.E. (eds) Industrial Structural Geology: Principles, Techniques and Integration. Geological Society, London, Special Publications, 421, 69–82.

McQuillan, H. 1973. Small-scale fracture density in Asmari Formation of Southwest Iran and its relation to bed thickness and Structural setting. AAPG Bulletin, 57, 2367–2385.

Nelson, R.A., 2001. Geological analysis of naturally fractured reservoirs. Second Edition. Gulf Professional Publishing, Houston. 332.

Nemati, M., Pezeshk, H., 2005. Spatial distribution of fractures in the Asmari Formation of Iran in subsurface environment: Effect of lithology and petrophysical properties. Natural Resources Research, 14, 305–316.

Price, N., 1966. Fault and Joint Development in Brittle and Semi-Brittle Rock. Pergamon Press, Oxford. 176.

Price, N., Cosgrove, J., 1990. Analysis of geological structures. Cambridge University Press, Cambridge. 502.

Priest, S.D., 1993. Discontinuity Analysis for Rock Engineering. Chapman & Hall, London. 473.

Reif, D., Decker, K., Grasemann, B., Peresson, H., 2012. Fracture patterns in the Zagros fold-and-thrust belt, Kurdistan Region of Iraq. Tectonophysics 576-577, 46–62.

Reif, D., Grasemann, B., Faber, R.H., 2011. Quantitative structural analysis using remote sensing data: Kurdistan, northeast Iraq. AAPG Bulletin 95, 941–956.

Sadooni, F.N., 1995. Petroleum prospects of Upper Triassic carbonates in northern Iraq. Journal of Petroleum Geology 18, 171–190.

Sissakian, V.K., Hagopian, D.H., 1995. Geological map of A-Mosul quadrangle, Sheet NJ-38-13, Scale 1: 250 000, GEOSURV, Baghdad, Iraq.

Sissakian, V.K., 1997. Geological map of Erbil and Mahabad quadrangles, Sheets NJ-38-14 and NJ-38-15, Scale 1: 250 000, GEOSURV, Baghdad, Iraq.

Sissakian, V.K., 2013. Geological evolution of the Iraqi Mesopotamia Foredeep, inner platform and near surroundings of the Arabian Plate. Journal of Air Transport Management 31, 152–163.

Schlumberger, 2013. Techlog 2013.4.0. Grabels.

Sharp, I., Gillespie, P., Lønøy, A., Horn, S., Morsalnezhad, D., 2006. Outcrop characterization of fractured Cretaceous carbonate reservoirs, Zagros Mts, Iran. SPE Paper.

Stephenson, B.J., Koopman, A., Hillgartner, H., Mcquillan, H., Bourne, S., Noad, J.J., Rawnsley, K., 2007, Structural and stratigraphic controls on fold-related fracturing in the Zagros Mountains, Iran: implications for reservoir development. In: Lonergan, L., Jolly, R.J. H., Rawnsley, K., Sanderson, D.J. (eds) Fractured Reservoirs. Geological Society, London, Special Publications, 270, 1–21.

Talbot, C.J., Alavi, M. 1996. The past of a future syntaxis across the Zagros. In: Alsop, G.I., Blundell, D.J., Davison, I. (eds) Salt Tectoncs. Geological Society, London, Special Publications, 100, 89–109.

Tavani, S., Storti, F., Soleimany, B., Fallah, M., Muñoz, J.P., Gambini, R., 2011. Geometry, kinematics and fracture pattern of the Bangestan anticline, Zagros, SW Iran. Geological Magazine, 148, 964–979.

Tearpock, D.J., R.E. Bischke, 2003. Applied subsurface geological mapping: New Jersey, Prentice Hall, 822.

The MathWorks Inc., 2013. Matlab2013a. Natick, MA.

Terzaghi, R.D., 1965. Source of error in joint surveys. Geotechnique 15, 287–304.

Underwood, C.A., Cooke, M.L., Simo, J.A. & Muldoon, M.A. 2003. Stratigraphic controls on vertical fracture pattern I Silurian dolomite, northeasten Wisconsin. AAPG Bulletin, 87, 121–141.

van Bellen, R.C., Dunnington, H.V., Wetzel, R., Morton, D.M. 1959. Iraq. In: Dubertret, L. (ed.) *Lexique Stratigraphique International*, 3, *Asie*. CNRS, Paris, fasc 10a, 333.

Wennberg, O.P., Svånå, T., Azizzadeh, M., Aqrawi, A.M.M., Brockbank, P., Lyslo, K.B., Ogilvie, S., 2006. Fracture intensity vs. mechanical stratigraphy in platform top carbonates:

The Aquitanian of the Asmari Formation, Khaviz Anticline, Zagros, SW Iran. Petroleum Geoscience 12, 235–245.

Figures

Table 1: Studied fracture-forming events and available datasets from outcrops and subsurface.

Figure 1: (a) Tectonic map of the Iraqi Kurdistan. The study area is indicated by the black rectangular box (After Jassim and Goff, 2006); (b) Simplified Geological map of Kurdistan showing the anticlinal axes and related thrust faults. The studied anticlines are labelled (After Sissakian and Hagopian, 1995; Sissakian, 1997; Csontos et al., 2012).

Figure 2: Stratigraphy of the Upper Triassic and Jurassic in Kurdistan. The Kurra Chine Formation (Upper Triassic) and Sehkaniyan Formation (Lower Jurassic) are the studied fractured reservoir units. Note that Alan, Mus and Adaiyah formations are the subsurface equivalent of the Sehkaniyan Formation (After van Bellen et al., 1959; Csontos et al., 2012).

Figure 3: Observed fracture sets shown in Price's classification of fracture sets typical for asymmetric anticlines (after Price, 1966; modified from Price and Cosgrove, 1990). The hypothesis is that hinge-perpendicular fractures are pre-folding whereas hinge-parallel and oblique fractures are fold-related or post-folding fractures.

Figure 4: (a) Photograph looking east of crest of the Gara Anticline. Samples were collected from the Kurra Chine and Sehkaniyan formations at different structural positions; (b) Kurra Chine Formation at locality KC-3 (See Figure 5 for localities); (c) Thin cemented fractures with calcite in the Kurra Chine Formation; (d) Vugs (angular pores) in the Sehkaniyan Formation; (e) Partial cemented fracture with calcite and include some bitumen.

Figure 5: (a) Fracture strike orientations of the Kurra Chine and Sehkaniyan formations at different structural positions (i.e. forelimb, hinge, backlimb) in the Gara Anticline. Stereograms: Schmidt lower hemisphere; black dashed semi-circle is bedding plane. Both measured data sets (with fracture density diagram at the background) and back-tilted (unfolded) data sets (without density diagram at the background) are shown. Red solid semi-circle is hinge-parallel fractures. Blue solid semi-circle is hinge-perpendicular fractures. Green solid semi-circle is hinge-oblique fractures. Contour lines represent density of fracture population using Fisher distribution as contouring method. N is the number of fractures. The background is a simplified geological map of the Gara Anticline draped over a shaded relief topographic map; (b) Cross-section of the Gara Anticline constructed only from the calculated dip angles using the constant dip domain method (Tearpock and Bischke, 2003). The grid reference of the northern end of the cross section is: Easting 370821; Northing 4100890; and southern end: Easting 369080; Northing 4088280; UTM Zone: 38N.

Figure 6: (a) and (b) Helium porosity versus nitrogen permeability of the Sehkaniyan and Kurra Chine formations measured from core plugs of samples that have been collected at Gara, Ora and Ranya anticlines; (c) and (d) Helium porosity versus nitrogen permeability of the Sehkaniyan and Kurra Chine formations measured from core plugs of samples that have been collected at the Gara Anticline. The dataset has been classified according to the structural position of the anticline.

Figure 7: (a) Fracture strike orientations of the Kurra Chine Formation at the forelimb of the Ora Anticline. Stereograms: same key as in Figure 5. The background is a simplified geological map of the Ora Anticline draped over a shaded relief topographic map; (b) Schematic cross-section of the Ora Anticline showing the steep forelimb and gentle backlimb. The grid reference of north end of the cross section: Easting 352744; Northing 4132427; and south end: Easting 348680; Northing 4120600; UTM Zone: 38N.

Figure 8: (a) Fracture strike orientations of the Sehkaniyan Formation at the forelimb of the Ranya Anticline. Stereograms: same key as in Figure 5. The background is a simplified geological map of the Ranya Anticline draped over a shaded relief topographic map; (b) Cross-section of the Ranya Anticline constructed only from the calculated dip angles using the constant dip domain method (After Reif et al., 2011). The grid reference of NE end of the cross section is: Easting 489770; Northing 4018030; and SW end: Easting 483055; Northing 4012539; UTM Zone: 38N.

Figure 9: Fracture intensity of the Sehkaniyan and the overlying Sargelu Formation measured at different localities in the Ranya Anticline. Fracture intensity is markedly higher in Sargelu thin bedded limestones than the underlying Sehkaniyan massive dolomites.

Figure 10: High confining pressure permeability data of the (a) Sehkaniyan and (b) Kurra Chine formations measured from core plugs of samples that have been collected at Gara, Ora and Ranya anticlines.

Figure 11: (a) Stereograms showing poles to planes and area-weighted rose diagrams of the conductive, resistive and hybrid fractures and faults of the Sehkaniyan Formation (Jurassic) in wells SH-1 and SH-2 and the Kurra Chine Formation (Triassic) in well SH-4 interpreted from borehole image logs (FMI and XRMI) in the Shaikhan Field. Dominant hinge perpendicular N-S fracture trends are observed in wells SH-1 and SH-2, whereas dominant hinge parallel WNW-ESE and a less dominant N-S fracture orientations were observed in well SH-4. Most fractures in this well were interpreted in the damage zones of WNW-ESE striking faults and hence fracture orientations are parallel to the fault trends in well SH-4. The same structural features were interpreted from borehole image logs (FMI and XRMI) in the Swara Tika Field. Dominant N-S and NNE-SSW fracture trends were observed in wells ST-1 and ST-2, respectively; The background is a simplified geological map; (b) Schematic

regional cross-section of NW Kurdistan across Gara, Swara Tika and Shaikhan anticlines (After de Verteuil et. al., 2011).

Figure 12: (a) and (b) Porosity versus P-wave acoustic velocity of the Sehkaniyan and Kurra Chine formations measured from wireline logs in well SH-1 of Shaikhan Field; (c) and (d) Porosity versus P-wave acoustic velocity of the Sehkaniyan and Kurra Chine formations measured from wireline logs in well ST-1 of Swara Tika Field. All the datasets are distributed between Voigt upper bound and Reuss lower bound. See text for explanation.

Figure 13: (a) and (b) Porosity versus acoustic velocity of the Sehkaniyan and Kurra Chine formations measured from core plugs of dry outcrop samples that have been collected at Gara, Ora and Ranya anticlines; (c) and (d) The same datasets have been classified according to the structural positions of the anticlines.

Figure 14: Schematic cartoon of a pericline illustrating the actual fracture results on the Gara, Shaikhan and Swara Tika anticlines. This conceptual fracture model may be applicable to other anticlines in Kurdistan, especially where the fracture patterns, fold morphology and structural style are similar to the studied structures. The pericline cartoon is modified from Fossen (2010).

Study area	Studied fracture-forming variables	Available datasets
Gara Ora Ranya	Structural position Lithological variation Petrophysical properties Burial and overburden removall Proximity to faults	Fracture orientation, spacing, intensity (P10), length, type.. Porosity, permeability, acoustic velocity, confining pressure permeability
Shaikhan Swara Tika	Lithological variation Petrophysical properties Proximity to faults	Fracture orientation, spacing, intensity (P10), type.. Porosity, acoustic velocity, elastic properties

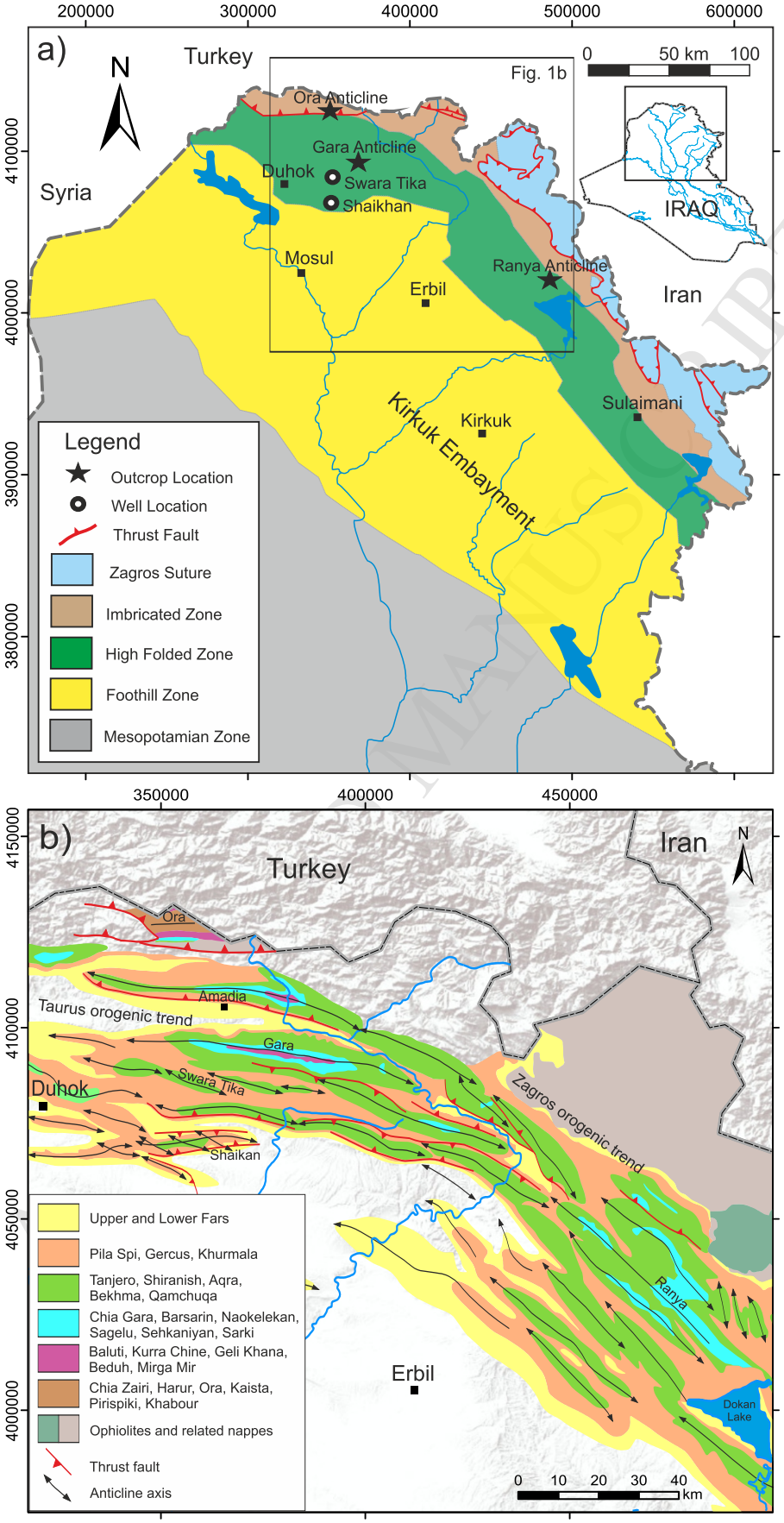

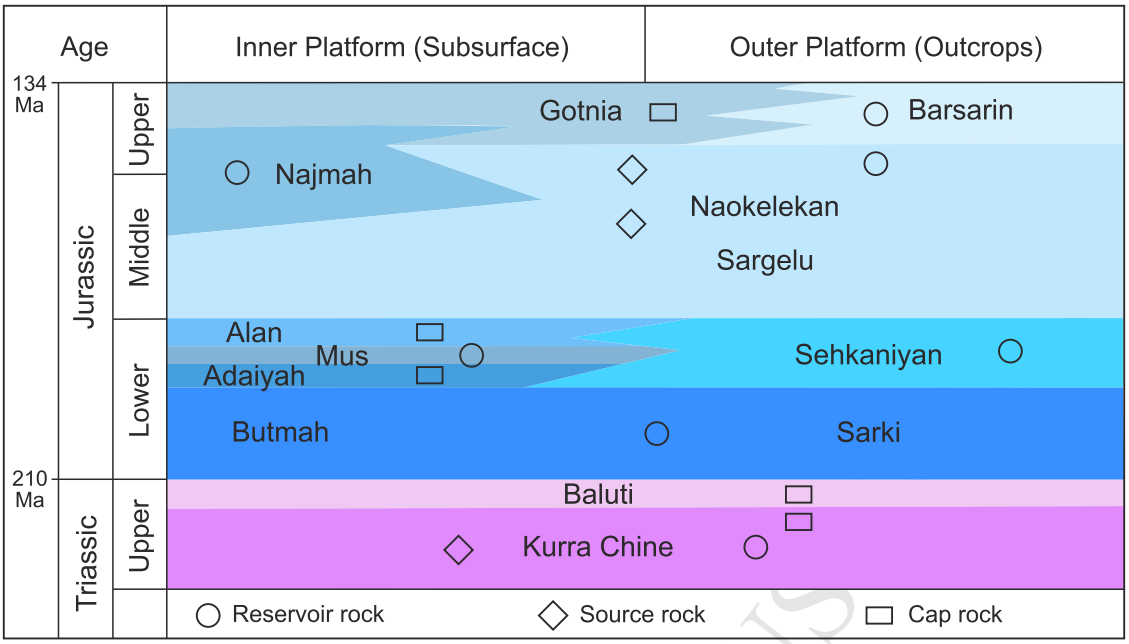

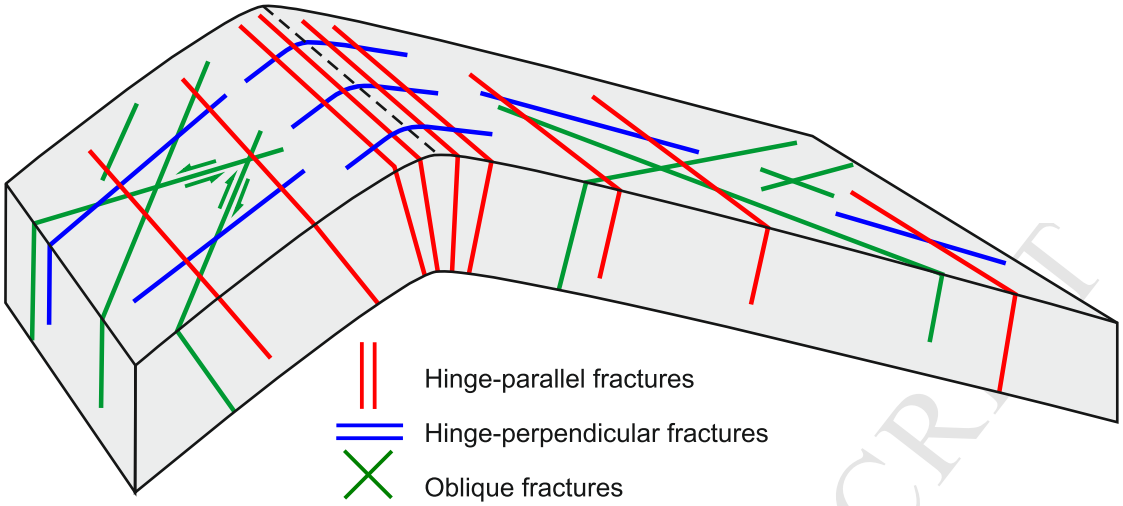

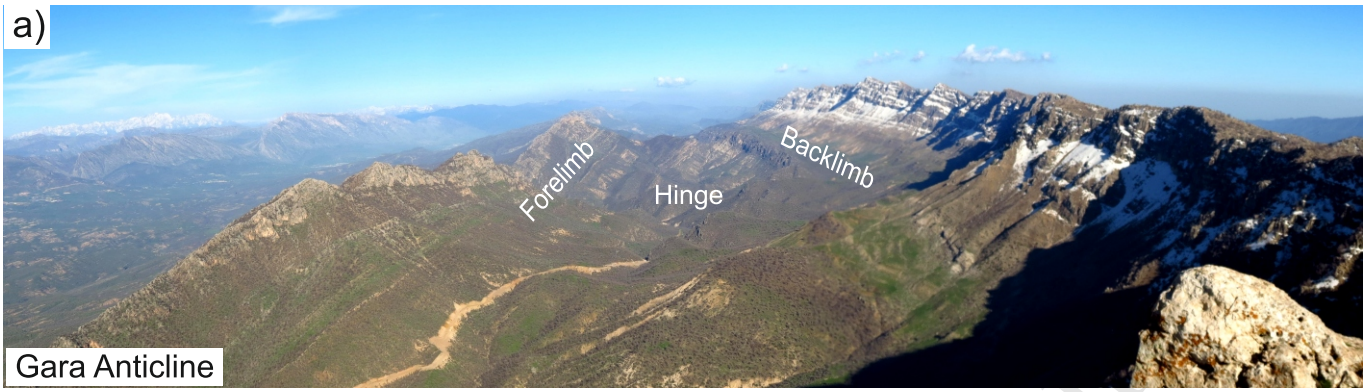
a)
Forelimb
Hinge
Backlimb
Gara Anticline

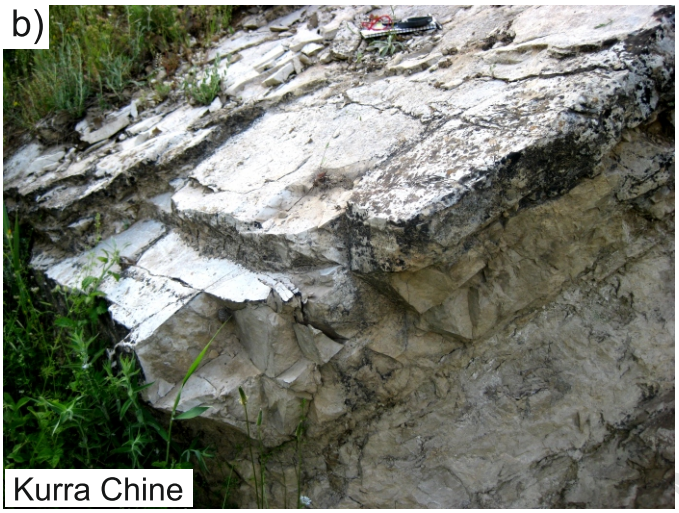
b)
Kurra Chine


d)
Sehkaniyan

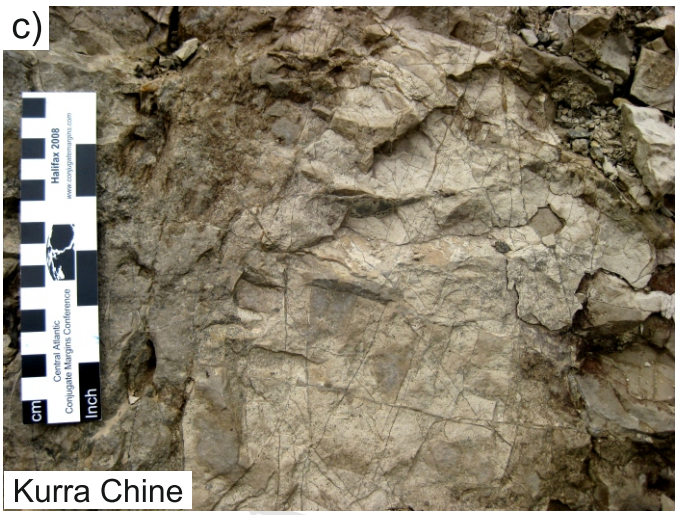
c)
Halifax 2008
Central Atlantic Conjugate Margins Conference
cm
inch
Kurra Chine


e)
Sehkaniyan

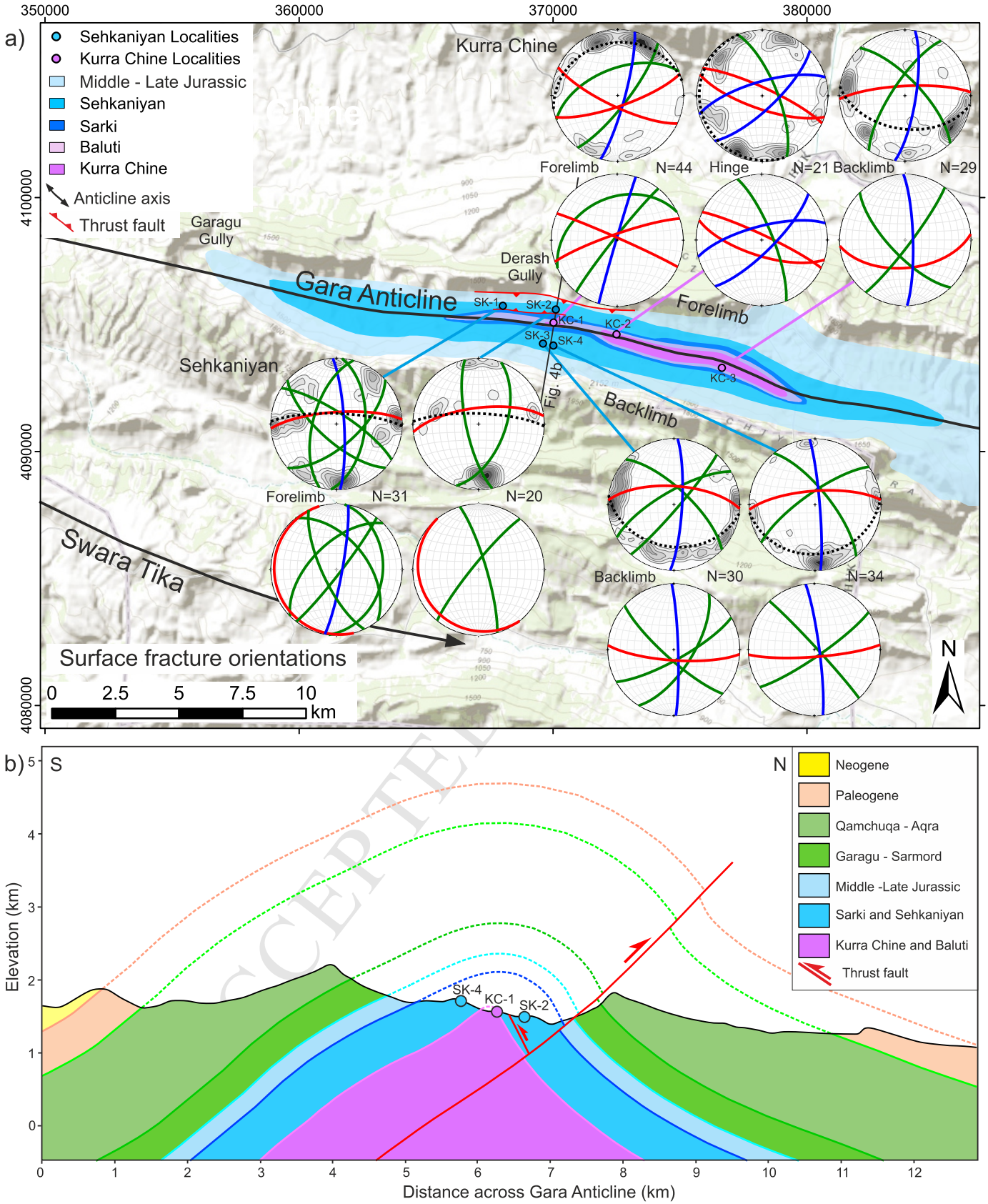

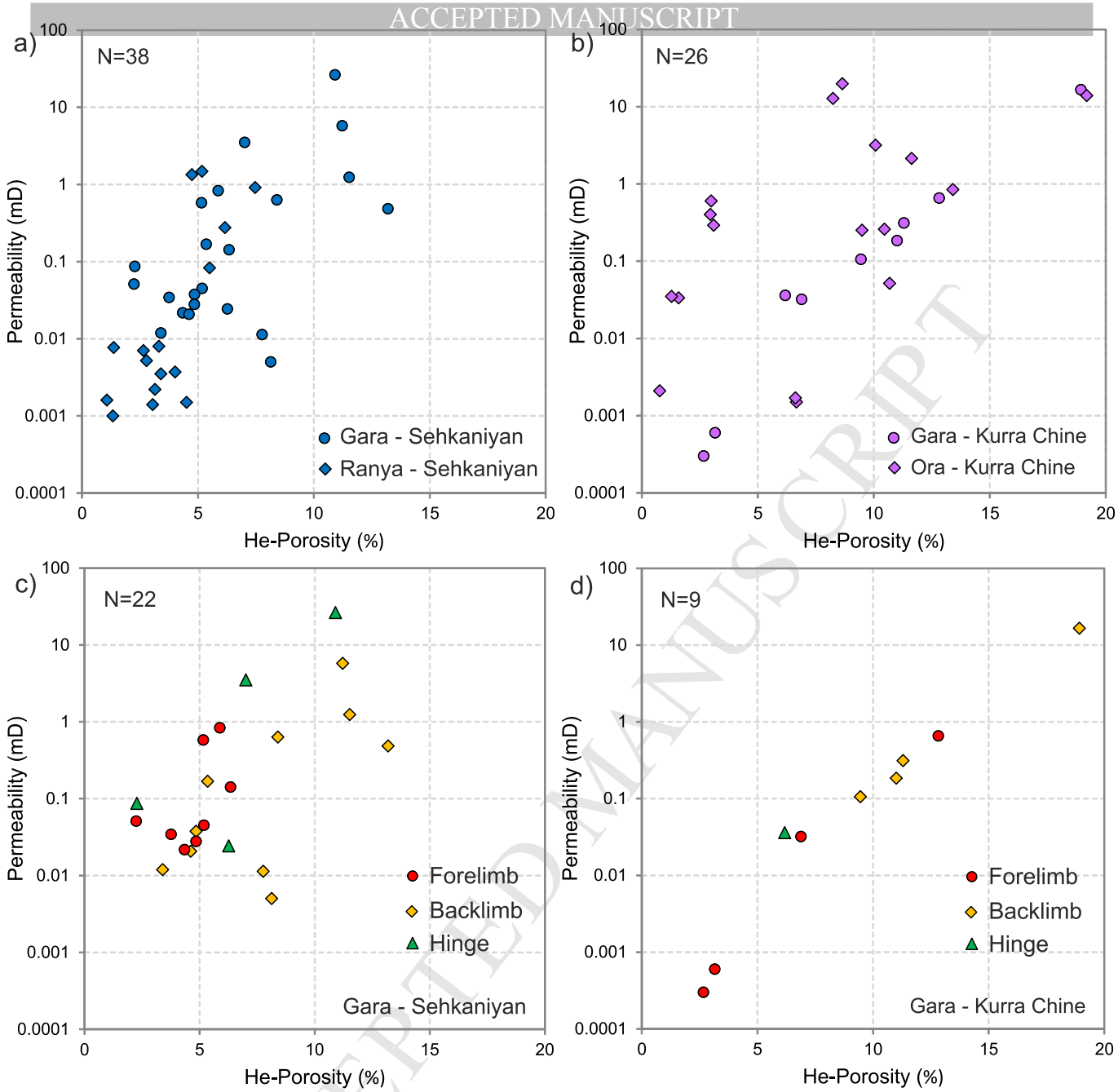

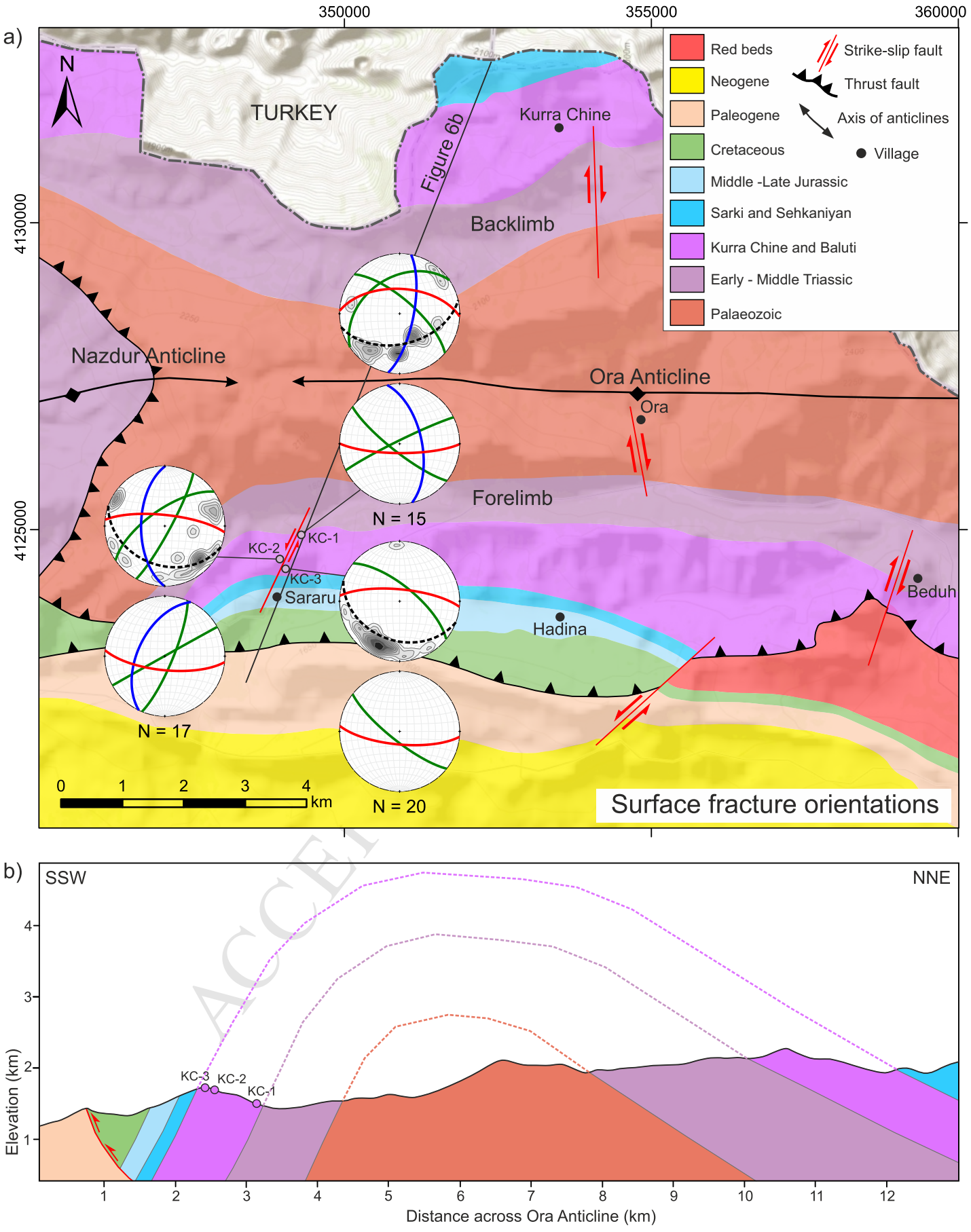

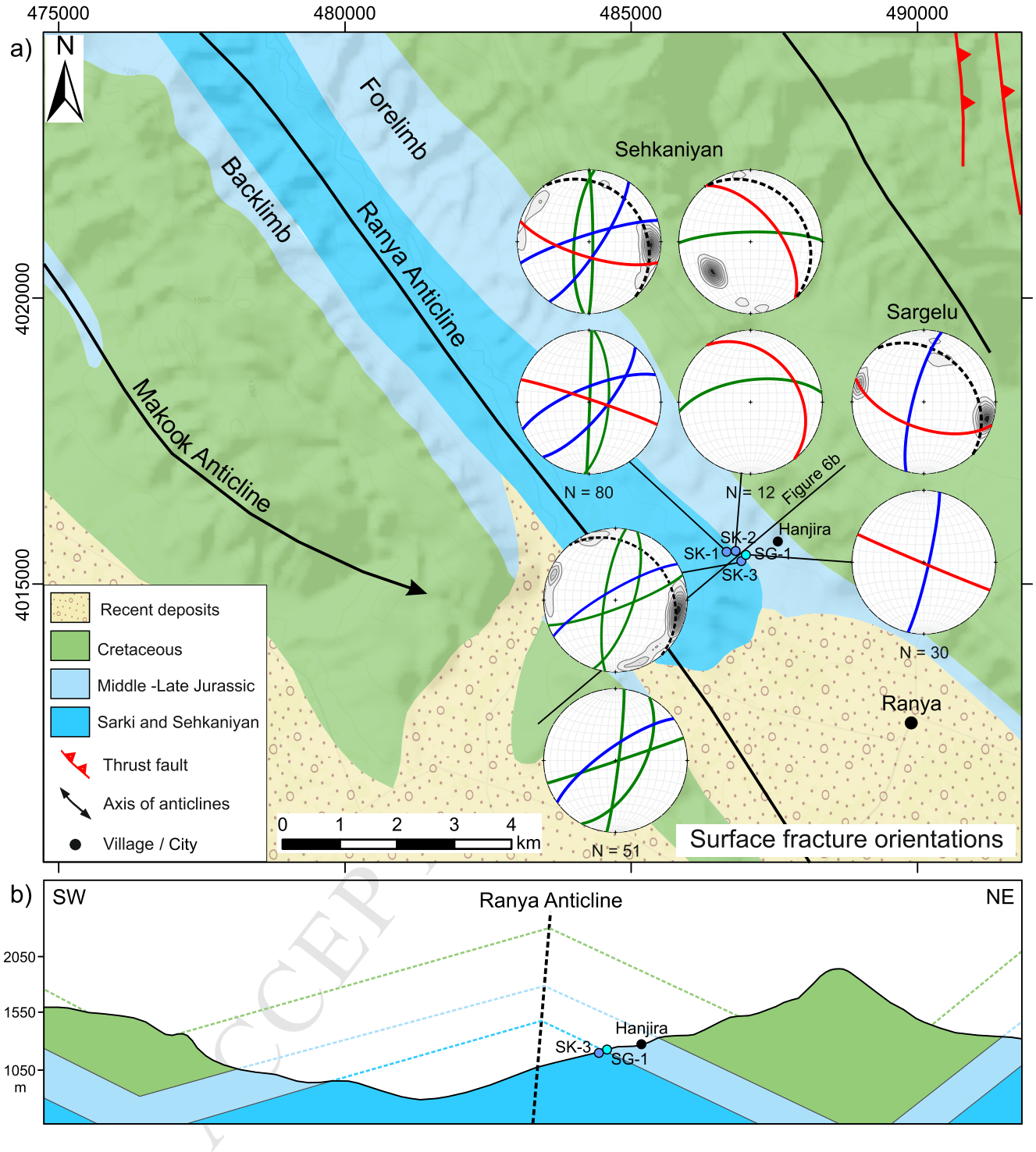
475000
480000
485000
490000
a)
N
4020000
4015000
Forelimb
Backlimb
Ranya Anticline
Makook Anticline
Sehkaniyan
Sargelu
N = 80
N = 12
Figure 6b
Hanjira
SK-2
SK-1
SG-1
SK-3
N = 30
Ranya
N = 51
Recent deposits
Cretaceous
Middle -Late Jurassic
Sarki and Sehkaniyan
Thrust fault
Axis of anticlines
Village / City
0 1 2 3 4
km
Surface fracture orientations
b)
SW
Ranya Anticline
NE
2050
1550
1050
m
Hanjira
SK-3
SG-1

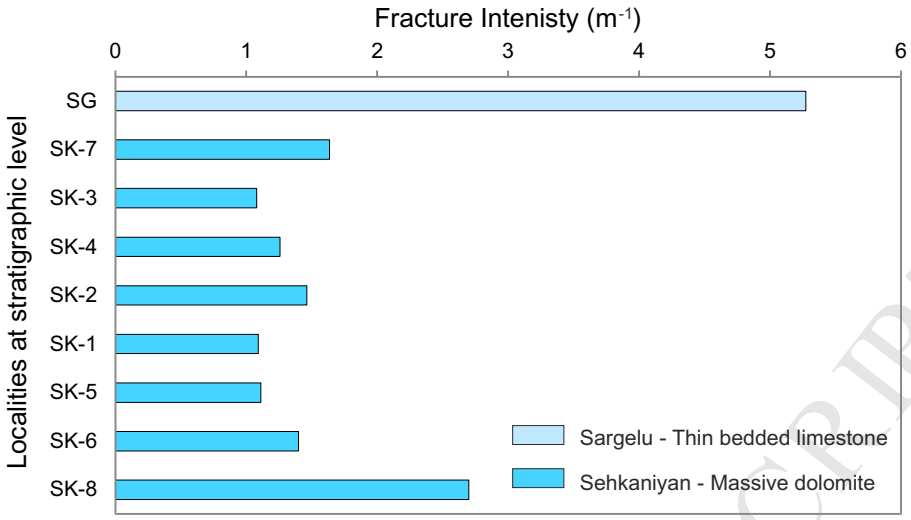

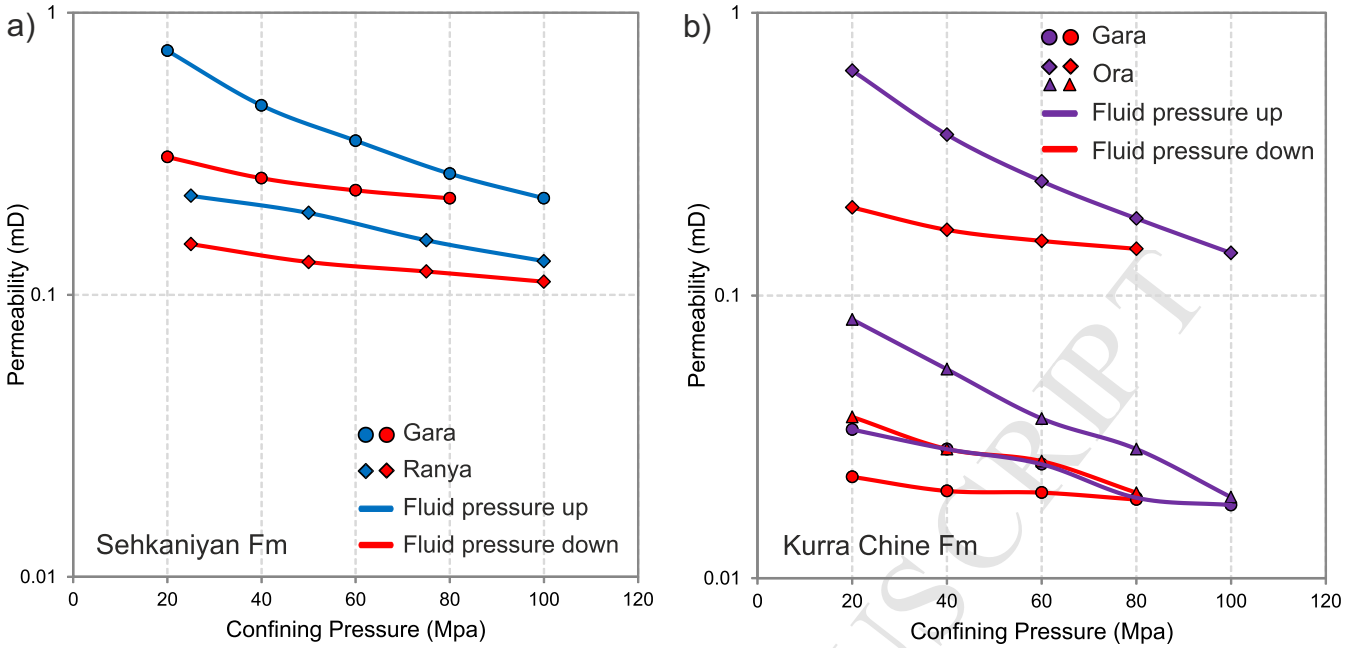

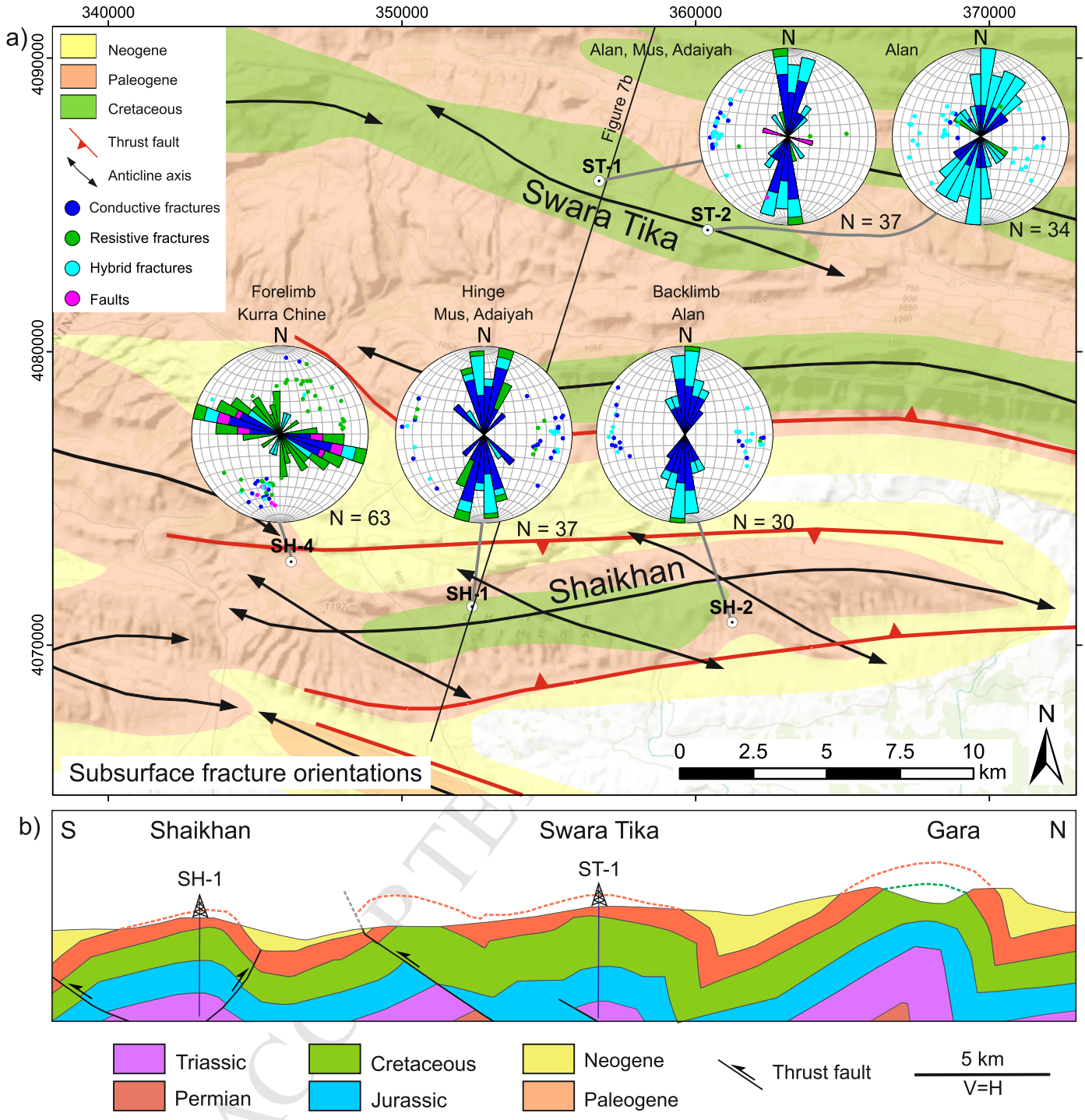

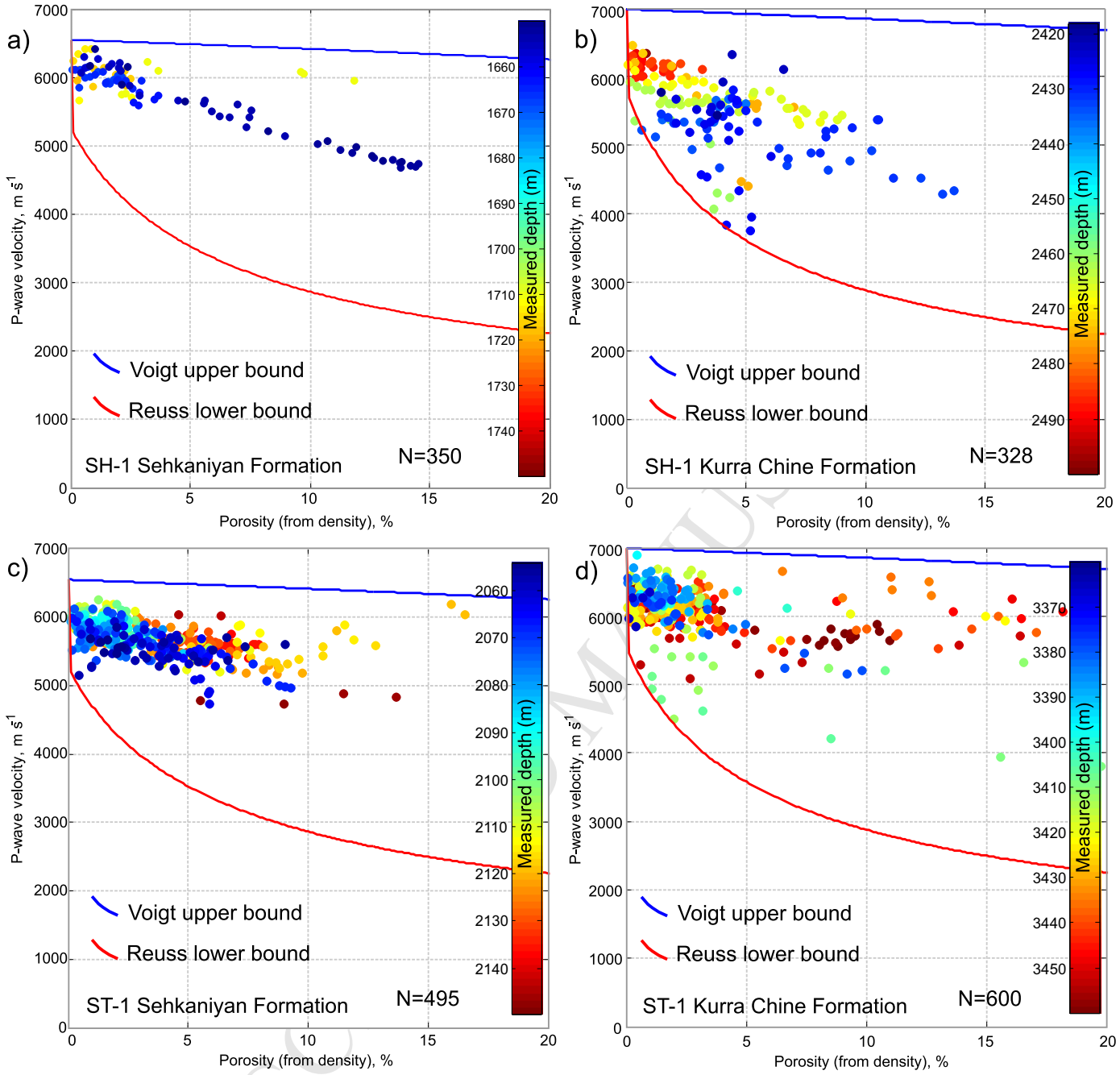

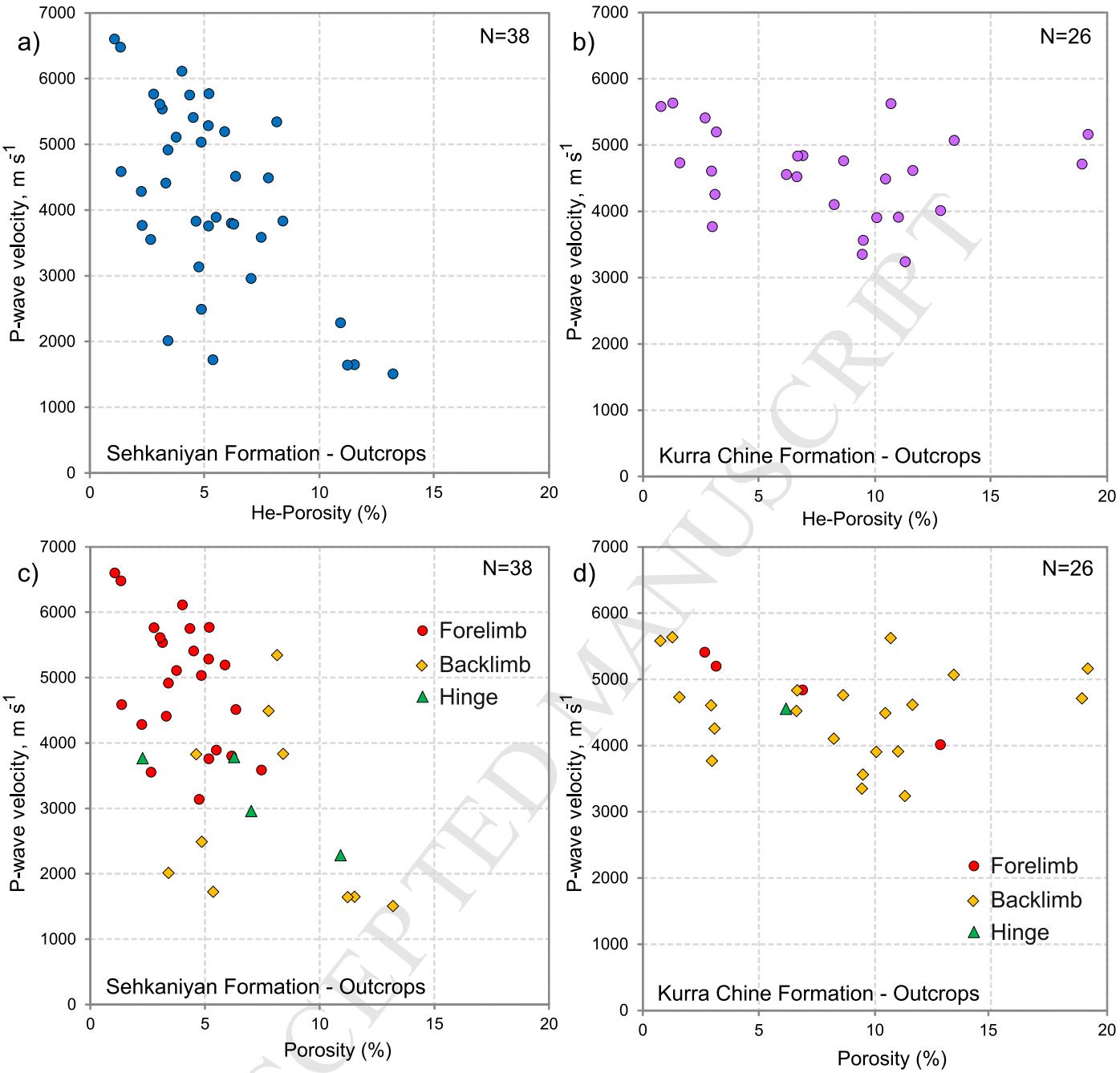

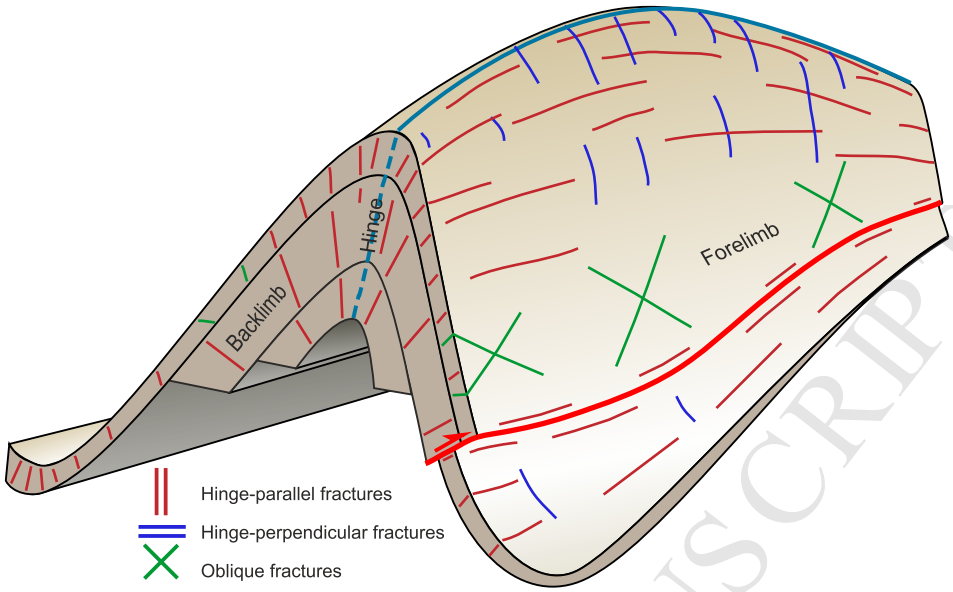

Highlights

- Fractures may show relationships to local folding, faulting and *in-situ* stress
- Fracture intensity may be influenced by lithology and bed thickness
- Petrophysical properties are influenced by lithology, position on folds and faults